Tissue-specific adaptation of human T cells is preserved during tissue inflammation

Nicole B. Potchen[1], Hugh R. MacMillan[1], Eva Domenjo-Vila[1], Andrew J. Konecny[1,2], Alexis K. Taber[1], Caitlin S. DeJong[1], Geervani Daggupati[1,2], Swati Shree[3], Stephen A. McCartney[3], Shelton W. Wright[4], Evan W. Newell[1,6], Douglas R. Dixon[5], Martin Prlic[1,6*]

[1] Vaccine and Infectious Disease Division, Fred Hutchinson Cancer Center, Seattle, WA, USA.

[2] Department of Immunology, University of Washington, Seattle, WA, USA.

[3] Division of Maternal Fetal Medicine, Department of Obstetrics and Gynecology, University of Washington, Seattle, WA, USA.

[4] Division of Pediatric Critical Care Medicine, Department of Pediatrics, University of Washington, Seattle, WA, USA.

[5] Department of Bioscience Research and Periodontics, University of Tennessee Health Science Center, College of Dentistry, Memphis, TN, USA.

[6] Department of Global Health, University of Washington, Seattle, WA, USA.

* Corresponding author

Fred Hutchinson Cancer Center, Vaccine and Infectious Disease Division, Seattle, WA, USA.

mprlic@fredhutch.org

Summary

T cells play an essential role in protecting tissues against pathogens and regulating tissue homeostasis. Previous studies highlight that T cells display tissue-specific phenotypic and functional properties, suggesting that T cells adapt to their local environment. Whether inflammation disrupts tissue-specific T cell adaptation remains poorly understood. To address this open question, we examined the T cell compartment – including conventional CD4 and CD8 T cells, regulatory T cells, γδ T cells, and MAIT cells – from healthy and inflamed human mucosal tissues. Using high-parameter spectral flow cytometry, we examined phenotype *ex vivo* and the functional capacity following stimulation, utilizing conventional gating and unsupervised clustering analysis approaches. Overall, we analyzed 65 tissue samples including mild, moderate, and severely inflamed oral gingiva, healthy and inflamed lung, along with healthy and inflamed tissue from the decidual-placental interface. Across these mucosal barrier tissues, we find that tissue location plays a dominant role in shaping the composition, phenotype, and functional capacity of the T cell compartment. Importantly, these tissue-specific adaptations were largely maintained during states of tissue inflammation. This included the ability to exert tissue repair functions, which was preserved across T cell subsets, even in severely inflamed tissues.

Introduction

Human T cells have distinct phenotypic and functional properties across different tissues and organs. This was initially demonstrated by Farber and colleagues who examined the phenotype and functional properties of conventional CD4 and CD8 T cells isolated from secondary lymphoid tissues, lung, jejunum, ileum and colon of trauma-induced, deceased organ donors[1]. This study furthermore established CD69 expression as a biomarker for tissue-residence for human CD4 T cells, and CD69 and CD103 co-expression to indicate tissue-residence for CD8 T cells[1]. Follow-up studies highlighted that expression of CD69 by human CD4 and CD8 T cells is associated with a core transcriptional signature akin to bona fide murine tissue-resident T cells[2]. Human tissue-resident memory CD8 T cells (T_{RM}) show tissue-specific adaptation such as distinct cytotoxic properties across skin, lung, and jejunum, and are also clonally distinct across these tissue sites[3-7]. A recent study indicated that within the intestine, distinct tissue niches drive unique phenotypic and functional properties in CD8 T cells, thus providing further compelling evidence that T_{RM} tissue location and functional state are fundamentally linked[8]. Similarly, conventional CD4 T cells (CD4 Tconv) and regulatory T cells (CD4 Treg) also have distinct phenotypic and functional properties across tissues[9-12]. Further evidence points to innate-like T cells also adapting in a tissue-specific manner. Human $\gamma\delta$ T cells differ by tissue location with cells from adult lung, spleen, lymph nodes (LNs), and gut tissue clustering differentially by tissue based on their expression of transcripts associated with effector and repair functions[13]. Finally, human mucosal-associated invariant T (MAIT) cells across tissues have distinct T cell receptor (TCR) repertoires and cytokine expression profiles[14,15].

Whether tissue-specific adaptations are maintained during tissue inflammation is unclear. Inflammation involves coordinated immune cell recruitment and activation and thus has the potential to profoundly alter the T cell compartment within tissue[16]. Memory phenotype CD8 T cells can be activated by pro-inflammatory signals alone; this event has been coined bystander-

62 activation or inflammation-driven activation of T cells[17,18]. Inflammation-driven activation of
63 memory CD8 T cells leads to increased expression of CD69, PD-1, and TOX, along with
64 expression of IFNγ and Granzyme B (GzmB)[19-23] which can have protective properties[24,25] but can
65 also lead to tissue pathologies[26]. Such bystander-activated CD8 T cell-mediated pathology has
66 been demonstrated in a human cohort following infection with Hepatitis A virus (HAV)[27]. For CD4
67 T cells, inflammation and associated tissue pathology is often associated with expression of IL-
68 17, but it is noteworthy that IL-17 should not be simply viewed as a pro-inflammatory cytokine[28]
69 or indicator of excessive inflammation[29]. Importantly, in addition to mediating tissue protection and
70 pathology, T cells also play a role in restoring tissue homeostasis via secretion of IL-22 and the
71 epidermal growth factor receptor (EGFR)-ligand amphiregulin (AREG)[30-32]. Tregs express AREG
72 in response to IL-18 and IL-33[33], while a recent study demonstrates that human memory CD8 T
73 cells express AREG in response to TCR stimulation[34].

74 While there has been substantial progress in our understanding of the T cell compartment
75 and its tissue-specific functional properties in healthy human tissues, the extent to which
76 inflammation alters these functional properties remains an open question. We sought to address
77 if inflammation overrides any tissue-specific T cell adaption in human tissues. Specifically, we
78 aimed to determine if inflammation alters the composition of the T cell compartment and
79 associated functional properties, and if it affects the ability of T cells to maintain their tissue-
80 regenerative functions. To accomplish this, we collected healthy and inflamed tissues from 3
81 distinct mucosal barrier sites: oral mucosa (gingiva), lung, and the decidual-placental interface
82 (DPI). We developed a high-parameter flow cytometry panel containing 37 markers to define the
83 composition, phenotype, and functional capacity of the T cell compartment: CD4 Tconv, CD4
84 Treg, CD8 CD103+ T_{RM} and CD8 CD103- circulating T cells, along with the innate-like MAIT and
85 γδ T cell subsets. Overall, we found that the composition, phenotype and function of the T cell
86 compartment was driven more by tissue location than inflammation, indicating that T cells largely

87 maintain their tissue-specific adaptations during inflammation. Our data emphasize the need to
88 assess and consider inflammation in a tissue-specific manner. Furthermore, our data highlight
89 that T cells maintain their tissue-regenerative capacity even in severely inflamed tissues, thus
90 pinpointing T cells as a therapeutic target to treat inflammatory diseases.

91 # Results

92 **The inflammation state in the oral mucosa has a modest effect on composition and**
93 **phenotype of the T cell compartment**

94 To determine the impact of inflammation on the mucosal T cell compartment, we first
95 examined phenotypic differences across mildly, moderately, and severely inflamed gingival
96 tissues. These tissues are discarded from routine surgeries and represent a wide range of
97 inflammatory states. We assigned clinically healthy gingival tissue and tissue with mild gingivitis
98 as "mild inflammation" since even clinically healthy tissue contains a baseline level of
99 inflammation, which may allow for constant immune surveillance[35]. Next, we assigned tissues
100 with pronounced gingivitis transitioning to periodontitis as "moderate inflammation" and those with
101 periodontitis as "severe inflammation". While gingivitis is reversible with proper dental hygiene,
102 periodontitis is an irreversible, chronic disease state without clinical intervention[36]. A full sample
103 list with clinical information can be found in Supplemental Table 1. A 37-color spectral flow
104 cytometry panel was utilized to examine phenotype (no stimulation) and functional capacity
105 (following stimulation) of the T cells isolated from gingival tissues (***Figure 1A****, panel and gating;*
106 *Supplemental Figure 1-2*). As a technical control, a PBMC sample from a single leukapheresis
107 donor was included in every flow cytometry experiment (*Supplemental Figure 3*).

108 We first examined the frequency of T cells (CD3+ cells) within the CD45+ cell compartment
109 and found no changes between mild, moderate, and severely inflamed gingival tissue (***Figure***
110 ***1B***). Of note, a small population of naïve T cells (CCR7+ CD45RA+) was present in each tissue
111 sample. These naïve T cells presumably stem from the blood that is inherently present in the
112 tissue vasculature. We excluded these naïve T cells from our manual gating analysis approach.
113 We further analyzed the T cell compartment by first defining innate-like T cell subsets within the
114 CD3+ population, followed by subsetting the remaining CD4 and CD8 T cells into conventional
115 CD4 T cells (CD4 Tconv), regulatory CD4 T cells (Treg), CD103+ (tissue-resident phenotype)

116 CD8 T cells and CD103- (circulating) CD8 T cells (*Supplemental Figure 1B*). We then assessed
117 if T cell subset composition is altered with inflammation. We observed stable frequencies of most
118 T cell subsets, including CD4 Tconv, CD4 Treg, and CD103+ CD8 T cells (***Figure 1C***). We noticed
119 a slight reduction in CD103+ CD8 T cells within the total T cell population ($p = 0.1026$), but a
120 significant increase in circulating CD103- CD8 T cells in severely inflamed tissue compared to
121 mild inflammation (***Figure 1D***).

122 We next examined if the expression of activation, co-stimulation, and exhaustion markers
123 change with inflammation severity. To visualize similarities and differences in expression of
124 multiple proteins across different tissues, we chose a heatmap-based approach to displaying
125 expression frequency. For each protein, the mean expression frequency is shown on all
126 heatmaps, and the median and data range for each protein are shown in *Supplemental Table 2.*
127 Within conventional CD4 and CD8 T cell subsets, we observed only few changes between mild,
128 moderate, and severely inflamed gingiva (***Figure 1E***). Pro-inflammatory cytokines can increase
129 the expression of CD69, PD-1, and GzmB by memory CD8 T cells [20], but we did not observe an
130 inflammation-associated increase of these proteins (***Figure 1E***). On the contrary, we noted
131 reduced expression of CD69 in both the CD8 CD103+ and CD103- populations in severely
132 inflamed compared to mildly inflamed tissues. In the CD4 Tconv population, there were no
133 differences in these phenotypic markers. In general, we observed relative phenotypic stability
134 across inflammation status within each T cell subset (*Supplemental Figure 4*).

135 Next, we examined innate-like T cell subsets including MAIT and $\gamma\delta$ T cells, which can
136 also be activated by pro-inflammatory stimuli[37,38]. While there were no statistically significant
137 differences in MAIT cell frequencies and phenotypic markers across inflammation status, we
138 found a significant reduction in $\gamma\delta$ T cells in severely inflamed compared to moderately inflamed
139 tissue (***Figure 1F***). Within the moderately inflamed condition, we also observed a pronounced
140 reduction of PD-1 expression in the $\gamma\delta$ T cell population (***Figure 1G***). The concomitant increase

141 in the abundance of γδ T cells (as a % of CD3+ T cells) and decreased PD-1 expression could
142 potentially be due to recruitment of γδ T cells from the blood to moderately inflamed tissue. While
143 we observed some phenotypic differences in our dataset as tissue became increasingly inflamed,
144 we noted that the T cell profile within all oral mucosal tissues remained overall rather stable even
145 in severely inflamed tissues. We next considered that a smaller proportion of T cells may respond
146 in a TCR-dependent manner.
147

148 **Biomarkers of TCR-mediated activation do not significantly change across inflammation**
149 **states in the oral mucosa**

150 We next assessed biomarker pairs indicative of TCR-mediated activation[39-41]. We
151 examined co-expression of CD39+ PD-1+ (for CD8+ cells[40,41]) as well as ICOS+ PD-1+ (for CD4+
152 cells[39]) across mild, moderate, and severely inflamed oral mucosal tissues. Across gingiva of
153 varying inflammation states, there were no differences in frequency of expression of each of these
154 populations. CD39, PD-1 and ICOS are also expressed on highly activated Tregs, and we
155 consistently observed the highest frequency of expression in CD4 Tregs (***Figure 2A-B***). In line
156 with this observation that TCR-mediated activation did not change across inflammation states, we
157 also observed no changes in Ki67 expression, an indicator of recent cell proliferation, across
158 inflammation status (***Figure 2C-D***). Lastly, we examined TIM3 and PD-1 expression, a biomarker
159 pair indicative of T cell exhaustion. We observed unaltered co-expression of these markers
160 regardless of inflammation state (***Figures 2C-D***). Together, these data indicate that biomarkers
161 of T cell activation and proliferation remained stable across a range of inflammatory disease
162 states within the gingiva. Overall, we did not detect evidence of inflammation- or TCR-driven
163 activation of the T cell compartment in the inflamed gingiva. To assess the ability of the T cells to
164 respond to activation we next interrogated T cell functional properties.
165

166 **Functional capacity for T cell-mediated tissue healing and cytokine production is**
167 **maintained in inflamed oral mucosa**

168 To examine if the functional capacity of T cell subsets varies across inflammation, we
169 stimulated T cells isolated from gingival tissue for 6 hours with PMA/ionomycin (***Figure 1A***). We
170 define the functional capacity simply as the ability of a T cell to express protein following this brief,
171 yet broad, activation stimulus. Within CD4 and CD8 subsets, we observed no statistically
172 significant differences in AREG, IFNγ, TNFα, IL-17A, IL-17F, IL-2, or IL-22 expression across
173 inflammation states (***Figure 3A****, Supplemental Figure 5*). Even the distribution of datapoints for
174 each T cell subset was similar across mildly, moderately, and severely inflamed gingiva (***Figure***
175 ***3B***).

176 Similarly, the functional capacity of MAIT and γδ T cells was stable across inflammation
177 states (***Figure 3C***). The mean, median, and data range are reported in Supplemental Table 2.
178 Within several T cell subsets, we found co-expression of GzmB and AREG upon stimulation,
179 which may indicate dual functional roles (cytotoxicity and tissue repair) can occur simultaneously
180 within the same T cell. The highest frequency of GzmB and AREG co-expression was observed
181 in CD8 CD103+ cells (***Figure 3D***), though these were also detected to a lesser extent in CD4
182 Tconv, CD4 Tregs, and innate-like subsets (~1% within CD4 Tconv, Treg and MAIT cells, ~4% in
183 γδ T cells). Overall, these data suggest T cell subsets retained their functional capacity even in
184 severely inflamed gingiva.

185

186 **T cells from lung and decidual-placental interference (DPI) differ based on tissue origin**
187 **regardless of inflammation status**

188 We next wanted to assess whether the phenotypic and functional stability of T cells across
189 inflammation states is a gingiva-specific phenomenon or could also be extended to other mucosal
190 tissues in healthy and inflamed states. We decided to examine the lung and the decidual-placental

191 interface (DPI) as a set of mucosal tissues that are inherently very distinct from the oral mucosa
192 in function and commensal exposure[42-44]. We assessed lung samples from deceased adult organ
193 donors (healthy) along with resected lung tissue from patients with interstitial lung disease (ILD).
194 Briefly, ILD is a group of pulmonary disorders causing inflammation and lung tissue scarring[45].
195 Tissue sampling was performed on both upper and lower lung lobes, which yielded nearly
196 congruent profiles (*Supplemental Figure 6*); the upper lobe data are shown for the remainder of
197 the figures. Decidual-placental interface (DPI) samples were taken from a cohort of term (37-41
198 weeks gestation), uncomplicated pregnancies (healthy) and a cohort of term pregnancies
199 diagnosed with intra-amniotic inflammation (IAI). IAI, often referred to as chorioamnionitis, is
200 typically an acute inflammatory response to a bacterial infection[46].

201 First, we examined the composition of the T cell compartment in lung and DPI (***Figure***
202 ***4A)***. T cells isolated from DPI tissues displayed a higher frequency of naïve cells among all CD3+
203 CD45+, which are likely derived from the highly vascularized placental tissue. These naïve T cells
204 were again excluded from manual gating analysis to facilitate a comparison with the memory
205 phenotype T cells in other tissues. We noted a decrease in MAIT cell ($p = 0.020$) and $\gamma\delta$ T cell (p
206 $= 0.133$) abundance in inflamed over healthy lung, but did not observe significant inflammation-
207 associated changes in the DPI (***Figure 4A)***.

208 Next, for each protein, the mean expression frequency is shown on all heatmaps in **Figure**
209 **4B**, Supplemental Figure 7, and the median and data range for each protein are shown in
210 Supplemental Table 2. We noted an inflammation-associated, statistically significant increase in
211 CD69+ T cells within CD4 Tregs, CD8 CD103+, and CD8 CD103- T cells in the placenta, but not
212 the lung (***Figure 4B****, Supplemental Figure 7, statistical analysis across tissues excluded from*
213 *heatmaps*). False discovery rate corrections for multiple comparisons of lung and placenta
214 phenotype were also performed (*Supplemental Table 3*). A profound inflammation-associated
215 phenotypic change occurred within T cells in the lung. We observed a dramatic reduction in CD25
216 expression on all T cell subsets in inflamed lungs (***Figure 4B***). Similarly to the oral mucosa, we

217 did not observe an increase in GzmB in healthy vs. inflamed tissues (lung and DPI) (***Figure 4B***),
218 and did not observe evidence for TCR-mediated activation, proliferation, or exhaustion
219 (*Supplemental Figure 8*). We next wanted to further quantify how tissue origin (lung and DPI) vs.
220 inflammation state affect protein expression of T cells. To accomplish this, we took the source of
221 variation from 2-way ANOVA statistical testing (row factor and column factor p values with $p <$
222 0.05). We observed that tissue origin had a greater impact on subset composition and phenotypic
223 differences than inflammation status. (*Supplementary Table 2, markers displayed on heatmaps*
224 *in Supplemental Figure 7*).

225 So far, the data indicate that tissue origin predominantly shaped the general phenotypic
226 profile of T cell subsets. We next combined all 3 tissue types for our subsequent analysis steps.
227 To further visualize this relationship of phenotype and tissue location vs. inflammation state
228 across all three tissue sets, we grouped all datapoints from each tissue (irrespective of
229 inflammation state), color-coded each datapoint according to inflammation state, and compared
230 the expression of T cell surface markers across gingiva, lung, and placenta within conventional T
231 cell subsets (***Figures 4C-E***). As highlighted in previous figures, we did not observe inflammation-
232 associated changes in GzmB expression in CD8 T cell subsets, however there was a significant
233 difference in GzmB expression in CD8 CD103- T cells in the gingiva compared to lung and DPI
234 (***Figure 4C***). Among these tissue sets, the gingiva is presumably the tissue that is most
235 consistently and substantially exposed to microbes and antigen yet still displayed the lowest
236 baseline GzmB expression in CD8 CD103- T cells. Similarly, the frequency of TIM3+ Tregs was
237 lowest in the gingiva (***Figure 4D***). TIM3 expression by Tregs is typically observed in highly
238 activated Tregs in the tumor microenvironment[47]. In our dataset, we observed a nearly 3x increase
239 in frequency of TIM3 expression in Tregs from the DPI compared to gingiva (***Figure 4D***).
240 Together, these data suggest that the DPI, although typically considered to be a sterile tissue
241 environment[42], shows signs of being concomitantly activated and suppressive. In line with this
242 notion, we also observed the highest frequency of CTLA4+ expressing CD8 CD103+ T cells in

243 the DPI (***Figure 4E***). Together, these data highlight that tissue-specific phenotypic adaptations
244 in the T cell compartment across these mucosal tissues were maintained during states of
245 inflammation. We next wanted to test if the functional capacity of these T cell subsets was similarly
246 maintained in all tissues during inflammation.
247
248 **Functional capacity of T cells is primarily shaped by tissue location**
249 As a first step, we examined the functional capacity of T cell subsets across lung and DPI
250 during health and disease. We found that the expression pattern of cytokines was relatively stable
251 across inflammatory states. Two statistically significant changes between healthy and inflamed
252 lung were noted in CD4 Tconv; a decrease in IL-17A and IL-17F expressing cells in inflamed
253 lungs (***Figure 5A****, Supplemental Figure 9, statistical analysis across tissues excluded from*
254 *heatmaps*). Full statistical testing (FDR corrections for multiple comparisons) is detailed in
255 Supplementary Table 3.
256 We next compared the functional capacity across all three tissue sites and inflammation
257 status, (***Figure 5B****, gingiva – top, circles; lung – middle, triangles; placenta – bottom, diamonds*).
258 These data highlight that the greatest capacity for T cell IFNγ production (***Figure 5B***, left panel)
259 and IL-2 (***Figure 5B***, middle panel) was observed in the DPI. TNFα was also produced in the
260 highest quantities by T cells from the DPI and lowest in the lung (***Figure 5C***). In contrast, IL-17A
261 expression was essentially absent in DPI T cell subsets and most prominent in the oral mucosa
262 (***Figure 5B***, right panel). Differences in the functional capacity of CD4 Tregs particularly stood out
263 (***Figure 5B).*** The oral mucosa contained a large fraction of Tregs that expressed IL-17A following
264 stimulation (***Figure 5B***, right panel), while Tregs from the placenta expressed IFNγ (***Figure 5B***,
265 left panel). Of note, we observed co-expression of IFNγ and IL-2 for both CD4 Tconv and Tregs
266 from the DPI (***Figure 5D***) thus potentially suggesting that some FoxP3+ CD127- T cells may be
267 activated CD4 Tconv (explored further in the discussion). Finally, it is noteworthy that the bias

268 towards certain functional properties in each tissue set was mirrored across several T cell
269 subsets. For example, gingival Tregs were the most potent IL-17 producers, and this was true for
270 CD4 T cell subsets, but also MAIT cells and γδ T cells (***Figure 5B***) regardless of inflammation
271 status. Overall, these data support the notion that the functional capacity of T cell subsets is linked
272 to tissue location, and that this can be maintained during inflammatory disease.
273

274 **Functional capacity of T cells across tissues and inflammation state by dimensionality**
275 **reduction analysis**

276 Our analysis approach so far was focused on specifically examining select biomarkers of
277 activation and functional properties**.** We next wanted to compare tissues in a more unsupervised
278 analysis approach. Of note, we performed this analysis separately for stimulated and unstimulated
279 samples. Stimulation – as expected – altered the expression of some cell surface biomarkers. We
280 reasoned that the presence vs. absence of stimulation-induced changes could also be informative
281 and included all phenotypic and functional markers in the antibody staining panel in this PCA
282 analysis (TIM3, CD39, ICOS, CD25, CD28, CD27, PD1, Ki67, IL1R1, CD137, CD40L, CTLA4, IL-
283 2, IL-22, AREG, IL-17A, IFNγ, GzmB, TNFα, IL-17F). We first used principal component analysis
284 (PCA) to compare the effect of tissue origin vs. inflammation status on T cell functional capacity
285 (***Figures 6A-D****, Supplemental Figure 10)*. Tissue-based differences in functional capacity were
286 particularly apparent in CD4 Tconv and CD8 CD103+ T cells (***Figures 6A-B***) and were somewhat
287 less pronounced in MAIT and γδ T cells (***Figures 6C-D***). In contrast, for all subsets, there was
288 near congruent clustering based on inflammation status.

289 When determining which parameters are contributing most to determining the principal
290 components (loading scores), upon stimulation, changes in IFNγ expression contributed the
291 greatest for all T cells. Differences in expression of the co-stimulatory molecules CD27 and CD28
292 were also significant contributors to the PCA. Importantly, similar findings were observed when

293 PCA was performed with unstimulated samples directly *ex vivo* (*Supplemental Figure 11)*. Taken
294 together, an unsupervised analysis approach further underlines the notion that tissue
295 inflammation is not sufficient to disrupt tissue-specific adaptation of the T cell compartment.
296

297 **An unsupervised analysis approach to compare the T cell compartment across tissues**
298 **and inflammation**

299 We next wanted to use an unsupervised approach to assess the relative abundance of T
300 cells with functional similarity across tissue and inflammation state. An unsupervised approach
301 also allows for discovery of phenotypically/functionally unique populations potentially missed by
302 manual gating of each marker using single- or double-positive gates. Of note, for this approach,
303 we included naïve T cells in the analysis as a reference population. Briefly, T cell subsets were
304 first defined by manual gating. We then performed scaling/normalization and defined global
305 clusters across all samples (described further in methods). We assessed each T cell subset using
306 this approach with tissues analyzed directly *ex vivo* and following stimulation. Given the profound
307 differences of Treg functional capacity between tissues, we first focused our analysis on
308 stimulated Tregs. We examined cluster frequencies across tissues (gingiva, pink; lung, green;
309 placenta, purple) (***Figure 7A***, *top row panels*) and across inflammation status (healthy, blue;
310 inflamed, red) (***Figure 7A,*** *bottom left panels*).

311 We next assessed the characteristics of the observed ten distinct population clusters using
312 a bubble plot (***Figure 7B***). The bubble plot highlighted that clusters 1 and 4 were comprised of
313 naïve cells based on the expression of CD45RA+ CCR7+, whereas the remaining clusters
314 consisted of memory subsets. The relative abundance of each cluster combined for all donors is
315 displayed in **Figure 7C**, and then further broken down by single donor in **Figure 7D**. Tregs that
316 expressed the cytokines IFNγ and IL-17A were in clusters 8 and 10, and – in line with our
317 observations from manual gating – most abundant in placenta and oral mucosa, respectively.
318 Overall, these data indicate that our manual gating analysis captured differences in Treg

319 functional capacity across tissues (***Figure 5B**, Supplemental Figure 9*). We next performed this
320 analysis for other T cell subsets. Clustering for CD4 Tconv cells across tissue and inflammation
321 is shown in *Supplemental Figure 12*; the results are also in line with our manual gating analysis.
322 To summarize all clustering data for other T cell subsets *ex vivo* and upon stimulation, we used
323 clustering frequencies to generate PCA plots (*Supplemental Figure 13-14*). When cluster
324 frequencies were used to determine principal components, distinct tissues (gingiva, lung, and
325 DPI) form unique groups, whereas healthy and inflamed tissues overlap. Overall, our
326 unsupervised analysis approach further highlights that clusters show tissue-specific
327 characteristics with minimal alterations due to inflammation status.

328 In summary, across all analysis methods, we found that tissue-specific adaptations of T
329 cell subsets were maintained during tissue inflammation.

330 ## Discussion

331 Our main goal was to assess the extent to which tissue-specific adaptation of the T cell
332 compartment is altered during tissue inflammation. We initially sought to address this question
333 by examining oral mucosal (gingiva) tissue, but subsequently extended our study to include
334 other mucosal tissues to ensure that our conclusions would not be limited to a single tissue. In
335 the gingiva, we observed that markers indicative of inflammation-driven T cell activation did not
336 significantly change in most T cell populations, including MAIT and $\gamma\delta$ T cells, as inflammation
337 severity of the gingiva increased. We considered that this could be due to the baseline level of
338 inflammation that is present even in healthy gingival tissues[35], which could yield unique
339 regulatory mechanisms in the tissue. Since the oral mucosa is colonized by a dynamic
340 microbiome and continuously exposed to dietary and microbial antigens[35], we also examined
341 the expression of biomarker pairs that indicate TCR-mediated activation. ICOS and PD-1, and
342 CD39 and PD-1 have been shown to be indicative of recent TCR activation for human CD4 and
343 CD8 T cells, respectively[39-41]. Neither of these biomarker pairs indicated an association of a
344 TCR-mediated T cell response in CD4 Tconv or a CD8 T cell subset gingiva with increased
345 severity in inflammation. Similarly, Ki67 expression, an indicator of cell proliferation, and
346 expression of PD-1 and TIM3, indictors of T cell exhaustion, did not change with increased
347 inflammation in the gingiva. Overall, our observations highlight that the overall composition and
348 the phenotypic properties of T cell subsets in the gingiva were largely maintained at various
349 states of inflammation.

350 Because of the unique physiological demands of the gingiva, including but not limited to
351 mastication, we asked if the T cell compartment would be similarly resistant to inflammation-
352 mediated changes in other mucosal tissues, specifically the lung and the decidual-placental
353 interface (DPI). CD4 Tconv and CD8 T cell subsets in the healthy lung did not express
354 biomarker pairs of TCR activation. However, in the DPI we found that a substantial fraction of

355 CD4 and CD8 T cell subsets co-expressed ICOS and PD-1, and CD39 and PD-1, respectively
356 (*Supplemental Figure 8*). These data could suggest that T cells in the DPI encounter their
357 antigen more frequently than T cell in the gingiva and lung. This could potentially be related to
358 the presence of fetal-derived, semi-allogenic tissue (the placenta is made of fetal-derived
359 trophoblasts) or could indicate that recently activated T cells migrate to the DPI to provide
360 protection. An in-depth analysis of the TCR repertoire in the DPI compared to other tissues may
361 provide a more definitive answer in future studies. Finally, ICOS, CD39 and PD-1 are all
362 expressed by highly activated Tregs, and expression of these markers was found on a large
363 fraction of Tregs across all tissues and inflammation states.

364 Given the presence of highly activated Tregs in all tissues, we explored whether Tregs
365 displayed functional differences. We found that in gingival tissues, regardless of inflammation
366 status, about 10% of Tregs expressed IL-17A. IL-17+ Treg have been previously described and
367 are thought to maintain their ability to suppress other T cells, while secreting IL-17 in response
368 to TCR-mediated activation, or IL-6 and IL-1β stimulation[48,49]. Importantly, both IL-6 and IL-1β
369 are expressed in healthy human gingiva[50,51]. In contrast, we did not observe IL-17+ Tregs in
370 lung or DPI. However, we found that a fraction of Tregs in both healthy and inflamed DPI could
371 express IFNγ, while none of the Tregs in other tissues expressed IFNγ following stimulation.
372 These cells could be Th1-like Tregs that have so far been mainly described in peripheral blood
373 in context of human autoimmune diseases and are thought to be hypo-suppressive[52]. Thus, our
374 observation could indicate that these Tregs also exist in a healthy human tissue (albeit from a
375 unique environment that contains a semi-allogeneic tissue), but it important to consider that
376 these could potentially be recently activated Th1 cells that temporarily express FoxP3[53-55].
377 Alternatively, these IFN γ^+ Tregs could be specialized to suppress Th1 responses as previously
378 shown in a mouse model system[56]. Follow up studies will be required to distinguish between
379 these possibilities and transcriptionally define this DPI-enriched Treg population. Overall, tissue-

380 associated phenotypes and functional properties were evident for Tregs, while inflammation-
381 associated changes were limited in our cross-tissue and inflammation-state comparison.

382 One of the most prominent phenotypic changes that we observed between a healthy and
383 inflamed tissue was the striking decrease in CD25 expression on T cell subsets in the inflamed
384 lung (Figure 4C, *Supplemental Figure 7*). Our PBMC batch control (*Supplemental Figure 3*)
385 allowed us to rule out technical reasons for these phenotype (wrong titer of the antibody, etc.).
386 Previous reports indicated an increase in serum soluble CD25 levels in individuals with ILD
387 (both granulomatous-lymphocytic and rheumatoid-arthritis associated ILD)[57,58]. ILD has also
388 been clinically associated with increased matrix metalloproteinase (MMP) expression in
389 serum[59,60], which cleaves CD25 from the surface of T cells. If there is a local increase in MMP
390 activity in ILD lungs, then this could provide an explanation of the decreased CD25 during ILD in
391 all T cell subsets.

392 We specifically looked for functional changes that have previously been associated with
393 inflammation status. Studies using gingival tissue indicated a potential association between
394 inflammation and the abundance of Th17 cells[61,62]. We found that the overall composition of the
395 T cell compartment, including the frequency of CD4 T cells that make IL-17A or IL-17F following
396 stimulation, is relatively stable even during inflammation. It is important to keep in mind that a
397 hallmark feature of inflammation is the recruitment of immune cell populations to a site of
398 inflammation, and that inflammation of the gingiva is associated with an increase in T cell
399 infiltration[63]. Thus, while the overall number of T cells with a specific function increases in
400 inflamed tissues, this is not necessarily associated with a skewing in functional properties within
401 the T cell compartment. Overall, the composition of the T cell compartment was consistent
402 between mildly to severely inflamed gingiva, with few subsets showing an increase or decrease
403 with inflammation. Specifically, we observed a reduction in resident CD8 CD103+ T cells within
404 more severely inflamed gingival tissue with a concomitant proportional increase in circulating

405 CD8 CD103- T cells. Of note, our study does not suggest that stability is always maintained.
406 This stable maintenance of function would presumably change, at least temporarily, in disease-
407 specific conditions with an associated antigen-specific T cell response, such as the Th17-driven
408 response against *Candida albicans* and *Staphylococcus aureus*[64].

409 Overall, a state of tissue inflammation does not per se override tissue-specific features
410 of the T cell compartment. Importantly, our observations for the T cell compartment do not
411 necessarily extend to inflammation-associated alterations of other cell types, particularly innate
412 immune cells, in these tissues. In the gingiva, it is well documented that neutrophil infiltration is
413 associated with acute inflammation[61,65,66]. In the lungs, similar innate subsets of macrophages
414 and neutrophils have been reported to drive inflammatory responses in mice and humans[67,68],
415 and acute chorioamnionitis has also been defined by neutrophil infiltration[69]. Again, it is
416 important to keep in mind that specific diseases can profoundly impact T cell phenotype and
417 function during inflammation. Thus, while our data indicate that tissue inflammation is not
418 inherently sufficient to override tissue-specific T cell adaptation, different disease settings may
419 display profound T cell changes such as previously observed in the context of Hepatitis A
420 infection, which leads to increased IL-15 availability and bystander activation of CD8 T cells[27].

421 Finally, we want to highlight that we used a brief PMA/Ionomycin stimulation condition to
422 examine the functional capacity of T cells. We reasoned that the broadly activating nature of this
423 stimulus will reveal which proteins T cell subsets are able to express, while keeping in mind that
424 it does not reveal which proteins are secreted in situ. This approach indicated that T cell subsets
425 retained their ability to express AREG even in chronically inflamed tissue such as the ILD lung
426 and severely inflamed gingiva. Whether AREG is actually secreted *in situ* by T cells to promote
427 epithelial cell recovery in the inflamed gingiva is unclear. CD8 T cells appear to require a TCR
428 signal to secret AREG[34] and given the lack of evidence for CD8 T cell activation (including TCR-
429 mediated T cell activation) in these tissues, *in situ* AREG secretion by CD8 T cells seems

430 unlikely. However, given that the functional capacity is maintained in inflamed tissues, novel
431 therapies could target AREG to elicit expression or other specific functional responses.

432 In summary, we report that T cells are able to maintain their tissue-specific core
433 identities during states of tissue inflammation. By gaining a more complete understanding of
434 how inflammation affects the tissue-specific T cell landscape, therapeutic approaches can be
435 designed to develop treatments to restore homeostasis with tissue-specific requirements in
436 mind.

437 # Material and Methods

438 ## Approvals & Study Population

439 *Tissue Samples and Protocols:* All protocols used in this study were approved by the Institutional
440 Review Board (IRB #0008335, 00008263, 00004036, 00001636). Signed informed consent was
441 obtained from all participants. A list of all samples, along with relevant clinical information can be
442 found in Supplementary Table 1. Each sample is from a unique donor.

443

444 *Oral Mucosa:* Oral mucosa samples were obtained from surgically discarded tissue from routine
445 surgeries, such as osseous surgery, functional or esthetic crown lengthening procedures, tooth
446 extractions, or impacted tooth uncover procedures. Mild inflammation (clinical health, mild to
447 moderate gingivitis), moderate inflammation (severe gingivitis, stage I, and stage II periodontitis),
448 and severe inflammation (stage III and IV periodontitis).

449

450 *Lung:* Healthy lung samples were redirected transplants from deceased organ donors. Donors
451 without history of lung disease, infection, and mechanical ventilation for >7 days were eligible for
452 screening. Inflamed lung samples (interstitial lung disease, ILD) were obtained from patients
453 undergoing lung transplant. Explant lungs and hilar lymph nodes were obtained from patients with
454 ILD undergoing lung transplant at the University of Washington.

455

456 *Decidual-Placenta Interface:* Both healthy and acutely inflamed (chorioamnionitis) third trimester
457 placentas were obtained following vaginal delivery or C-section, following labor or no labor
458 (detailed in Supplementary Table 1).

459

460 *Technical Control Sample:* A consistent leukopak peripheral blood mononuclear cell (PBMC)
461 sample was used throughout each flow cytometry batch and assessed alongside experimental

462 samples to ensure longitudinal control. Leukopak (4510-01 Ful Leuko Pack) obtained through
463 Bloodworks Bio (Seattle, WA).
464

465 **Isolation of Lymphocytes from Tissues**

466 *Oral Mucosa:* Following procedures, mucosal tissue was priority shipped overnight with cold
467 packs to Fred Hutch Cancer Center (FHCC). Upon arrival, tissue was washed with complete
468 media (RPMI1640 (11875-093, Gibco) with penicillin, streptomycin (15140-122, Gibco), and 10%
469 fetal bovine serum (FBS, PS-FB2, Peak Serum)). An optimized protocol was adapted from
470 reference[70], originally developed for processing solid tumors. Tissue was placed in a petri dish
471 and minced with a scalpel, then enzymatically digested (Collagenase II (C6885, Sigma-Aldrich),
472 DNAse (20 units/ml, #D502, Sigm) in complete media with reduced 7.5% FBS (RP7.5) in a 25 mL
473 volume at 37°C for 40 minutes while shaking. Following digest, the sample was passed through
474 a needle (16x1 ½ Blunt, 302833, BD) 10 times prior to passing through a 100-micron cell strainer.
475 Remaining tissue pieces were mashed using a syringe plunger, washed with complete media,
476 and frozen in 1 mL Recovery Cell Culture Freezing Medium (12648010, Gibco) and stored in
477 liquid nitrogen until future experiments. Cell viability and abundance were quantified prior to
478 freezing by staining a small sample aliquot (Guava antibodies 7-AAD, CD19, and CD45) for 15
479 minutes, resuspension in 1% PFA, and collection on the Guava easyCyte. Oral mucosa samples
480 in this study contained between 731-52,195 T cells, as analyzed by flow cytometry.
481

482 *Lung:* Lung tissue was processed in a similar fashion to the gingiva using the RP7.5 digestion for
483 50 minutes at 37°C while shaking at 225 RPM. Subsequently cells were washed with RP10,
484 strained through a 70μm filter and enumerated. Lung tissue samples contained between 1,537-
485 62,719 T cells.
486

487 *Decidual-Placenta Interface:* Tissue was processed as previously described[71]. Briefly, intact
488 placentas were biopsied up to a 0.5 cm depth on the maternal facing surface of the placenta
489 including both decidua basalis and placenta villi. Tissue was digested in digestion media (above)
490 and incubated at 37°C for 60 minutes with agitation. Concentration for digest was RP7.5 + 700
491 U/mL Collagenase Type II (Sigma-Aldrich) and 200 U/mL DNase. Cells were filtered and washed
492 with media. Red blood cells were removed using ACK lysis buffer, followed by resuspension with
493 media. Maternal blood was collected in tubes containing the anti-coagulant acid citric dextrose.
494 DPI tissue samples contained between 10,303-102,650 T cells.
495
496 *Technical Control Sample:* Leukopak was processed according to StemCell Technologies
497 protocol (https://www.stemcell.com/leukopak-processing-protocol.html). Two blood cell lysis
498 steps at room temperature and two platelet washes were performed prior to counting and freezing
499 20 million cells per aliquot.
500

501 **Stimulation Assay**

502 As briefly outlined in Figure 1A, upon experimentation, cryo-preserved single-cell suspension
503 isolated from tissues or blood (outlined above) were thawed in a 37°C water bath. 12,000 to 2
504 million cells per condition were plated in a U- or V-bottom 96 well plate in 200 uL complete media.
505 For assessing phenotype directly *ex vivo*, cells were left untreated for 2 hours at 37°C. GolgiStop
506 (Monensin, 554724, BD) and GolgiPlug (Protein Transport Inhibitor (Containing Brefeldin A),
507 555029, BD) were then added per manufacturer recommendations to compare directly to
508 stimulated samples and was returned to the 37°C incubator for 4 more hours (total of 6 hours).
509 During functional stimulation assays, samples were similarly thawed and plated. 200 uL complete
510 media supplemented with PMA (100 ng/mL, P8139, Sigma) and ionomycin (1000 ng/mL, I9657,
511 Sigma) for 6 hours, including the addition of Golgi stop/plug 2 hours after beginning the
512 stimulation. Upon completion, samples were stained for analysis by flow cytometry.

513

514 **Spectral Flow Cytometry**

515 *Staining:* For all experiments, upon completion of the assay, samples were stained previously
516 described[72]. Prior to experimentation, the spectral flow panel was tittered, optimized, and tested
517 to ensure proper design and maximal information could be obtained from each sample, as
518 detailed in reference[73]. All staining steps were performed in the dark at room temperature in a 96-
519 bottom plate. Cells were incubated with FcX block (422302, Biolegend) and Zombie NIR dye
520 (422302, Biolegend) in PBS (14190250, Gibco) for 15 minutes. Antibody master mixes were spun
521 down at 10,000xg for 4 minutes prior to staining to remove aggregates. Following live/dead
522 staining, cells were washed, following by surface staining in 50uL (antibody mix in PBS + 2% FBS
523 and 10% brilliant stain buffer (563794, BD)) for 20 minutes. Cells were then washed twice prior to
524 fix/perm (100 uL, 554722, BD) according to manufacturer guidelines for 30 minutes. After fixation,
525 cells were stained intracellularly for select markers noted in the panel (Supplementary Figure 1)
526 for 30 minutes, assembled in perm/wash buffe and 10% BSB. Finally, cells were washed twice
527 with perm/wash and resuspended in PBS + 2% FBS and stored at 4°C until acquisition the
528 following day on the BD Discover S8.

529

530 *Controls*: Single-stain controls were optimized for individual markers by staining either
531 unstimulated PBMCs, PBMCs following a 6-hour PMA/ionomycin stimulation, or unstimulated
532 control tissue samples (generally tonsil tumor infiltrate or regional lymph nodes). For two markers
533 expressed in low abundance in PBMC and tissue (IL-13 and IL-22), capture beads were used for
534 single-stain control. Control samples were taken through an identical staining protocol to
535 experimental samples, described above. A reference sample was also used within each
536 experiment as a longitudinal control (*Supplemental Figure 3*).

537

538 *Cytometer*: Data from all experiments was collected with the BD Discover S8 and the
539 FACSChorus software platform (BD Biosciences). The S8 is equipped with 5 lasers and 78
540 detectors. Compensation controls were prepared and used for each individual experiment, aside
541 from one run containing ILD 11 and 12. Upon collection, data was exported (FCS 3.1 format) and
542 analyzed using FlowJo version 10.10.0. Files were analyzed in batches by collection day, with
543 minor gating changes across different batches.
544

545 **Unsupervised Clustering**

546 Upon acquisition on the Discover S8 (BD), samples were gated (*Supplemental Figure 1*).
547 Following gating of time, lymphocytes, single cells, and live cells, T cells were gated (CD3+
548 CD45+) and exported as a new .fcs file in FlowJo. Files were also stripped of parameters out of
549 scope for this analysis, focusing on time, size channels, and those containing a fluorochrome
550 (*listed in Supplementary Figure 1*). Upon creation of files containing only T cells, separate streams
551 were created for each relevant T cell subset assessed in this study: $\gamma\delta$ T cells (TCR$\gamma\delta$+), MAIT
552 cells (CD161+ Vα7.2+), all CD4 (CD8-), Tconv (FoxP3-), Tregs (FoxP3+ CD127-), all CD8 (CD8+
553 CD4-), resident CD8 cells (CD103+), and circulating CD8 cells (CD103-). Naïve cells were
554 included in clustering analysis for all tissues.

555 We included additional samples in our clustering analysis as reference tissues for tissue-
556 enriched T cell subsets (*Supplemental Table 1, gray lines*). Lung and associated lymph nodes,
557 along with maternal blood from placental donors were included in multiple batches. We also
558 included tumor infiltrates from head and neck squamous cell carcinoma (HNSCC) and associated
559 lymph nodes. One experimental batch did not include marker CD127 and was excluded from the
560 Tconv and Treg clustering analyses (n = 1 pediatric lung and associated LNs, 2 inflamed lungs
561 and associated LNs, 2 tumor infiltrate samples, and 8 tumor associated LNs).

562 For each clustering stream, we used up to 20,000 T cells per sample. No minimum cell
563 threshold was utilized. Actual T cell counts for individual samples and primary clustering streams
564 were considered for count analysis. The following markers were used to develop clusters: CD161,
565 CD39, CCR7, ICOS, CD25, IL-17F, CD28, CD27, CD45RA, PD-1, Ki67, CD69, TIM3, IFNγ,
566 CTLA4, IL-13, IL-22, GzmB, TNFα, IL1R1, CD137, AREG, CD40L, IL-17A, CD45RO, IL-2.
567 Lineage markers and QC parameters were excluded from clustering analysis: CD3, CD45, CD4,
568 CD8, FoxP3, CD127 or CXCR5, CD103, TCRγδ, Vα7.2, Live/Dead, Autofluorescence. Spectre[74]
569 was used to determine appropriate arcsinh transformation values for each parameter.
570 Repeated clustering at the single cell level – necessary to identify and factor out technical
571 noise, or perceived batch effect – is computationally intractable at the scale of this study.
572 Therefore, within each of the streams, to arrive at globally defined clusters across all batches, we
573 cluster the centers of clusters from batch-specific clusterings[75,76]. Specifically, we 'over'-cluster
574 within each batch by first clustering, then subclustering the cells within each cluster. Next, we
575 compute the centroids of all (sub)clusters in each batch and cluster these (sub)cluster centroids
576 (or "metacells'' or "supercells") to arrive at a global (meta)clustering assignment for each metacell
577 from each batch[77]. At each stage we use the Rphenograph algorithm, with Leiden clustering of
578 shared nearest-neighbor graphs[78,79]. To address moderate drift across batches in some
579 parameters, we first align repeated control median transformed intensity values across batches
580 for select parameters, and next apply the same batch- and parameter-specific shifts to the
581 samples before metaclustering. We use Uniform Manifold Approximate Projection (UMAP) for
582 dimension reduction and data visualization within an iterative process of adjusting for perceived
583 batch effects, optimized by refining the metaclustering at a fixed Leiden resolution, before pushing
584 resolution higher[80].
585
586

587 **Statistical Analyses**

588 Statistical testing was performed using GraphPad Prism Software version 10.5. Testing us noted
589 within figure legends. All bar graphs represent the mean with standard deviation. Heatmaps
590 display the mean for each marker for a given sample group. For oral mucosa samples (*Figures*
591 *1-3*), significance was determined by testing using ordinary one-way ANOVA with Tukey's multiple
592 comparisons test. For lung and placenta data (*Figures 4-5*), 2-way ANOVA was utilized with
593 Tukey's multiple comparisons if comparing two tissues across inflammation states, or one-way
594 ANOVA if comparing with three tissues with grouped inflammation. All data using one-way
595 ANOVA was also assessed using the Benjamini-Hochberg false discovery rate (FDR) correction
596 with a rate of 10% and maintained statistical significance. Supplementary Table 2 used 2-way
597 ANOVA to compare lung and placenta across inflammation; the Benjamini-Hochberg FDR
598 correction with a rate of 10% was utilized.

599 ## Resource Availability

600 Raw flow cytometry files (.fcs) were submitted to ImmPort and assigned as Study SDY3484.

601 ## Acknowledgements

602 We thank the Flow Cytometry Shared Resources Core at Fred Hutch Cancer Center. We thank
603 M. Quinn Peters who provided and assisted with the R script used for PCA and Veronica Davé
604 who consulted on proper statical testing and corrections to be used for these analyses. We also
605 thank all members of the Prlic Lab for critical feedback and discussion.

606 ## Author contributions

607 Conceptualization: N.B.P., M.P. Methodology: N.B.P., H. R. M., M.P. Conducting experiments:
608 N.B.P., E. D. V., A. K. T., C. S. D., G. D. Formal analysis: N.B.P., H. R. M., M.P. Writing; original
609 draft: N.B.P., M.P. Writing; review and editing: all authors. Visualization: N.B.P., H. R. M., M.P.
610 Funding acquisition: N.B.P, M.P. Supervision: M.P.

611 ## Funding

612 NIH grants R56DE032009, R01AI123323 and R01AI179712 (to M.P) and funding from the Oral
613 Mucosa Immunology Consortium at the University of Nebraska (to N.B.P, Windsweep Farm
614 Scholar) supported this work.

615 ## Declarations of interest

616 The authors declare no competing interests.

617 ## Supplemental Information

618 Document S1. Figures S1-S14.

619 Tables S1-3 contain tissue information, data range of heatmaps, and statistical testing.

620 # Figure Legends

621 **Figure 1: Inflammation in the oral mucosa modestly affects composition and phenotype of**
622 **the T cell compartment.**

623 **A.** Experimental layout, described in detail in methods. Briefly, oral mucosa tissue of varying
624 inflammation states was sent from the clinic to lab, kept at 4°C. Tissue was digested mechanically
625 and enzymatically prior to storage of cryovials with single cell suspension in liquid nitrogen. Upon
626 experiment, samples were thawed and assessed directly ex vivo (*Figures 1-2*) or following a 6h
627 PMA/I stimulation at 37°C (*Figure 3*). **B.** Frequency of CD3+ T cells of CD45+ cells across
628 inflammation state, pre-gated on lymphocytes, single cells, and live (*Supplementary Figure 1*). **C.**
629 Of CD3+ CD45+ cells, frequency of each T cell subset. **D.** Frequency of subset (left to right,
630 CD8+ CD103+ resident, and CD8+ CD103- circulating) of CD3+ CD45+ T cells across
631 inflammation state. For **B-D.** T cell subsetting, n = 9 mild, 13 moderate, 11 severely inflamed oral
632 mucosa tissues. **E.** For each conventional subset, heatmaps depict frequency of activation
633 markers across inflammation status. Phenotyping of T cell subsets must meet minimum 25 cell
634 threshold; sample size is consistent with above unless noted; n = 8 mild, 11 moderate for Tregs.
635 Tconv, CD103+ and CD103- all met minimum threshold. **F.** Frequency of MAIT cells and $\gamma\delta$ T
636 cells of CD3+ CD45+ T cells. **G.** For innate-like T cells, frequency of activation markers across
637 inflammation. Minimum threshold of 25 cells; n = 7 mild, 9 moderate for MAIT cells; n = 8 mild for
638 $\gamma\delta$ T cells. For all plots, ns (not significant), *$p < 0.05$, ***$p < 0.001$, ****$p < 0.0001$ by ordinary
639 one-way ANOVA with Tukey's multiple comparison test.

640

641 **Figure 2: Biomarkers of T cell receptor (TCR)-mediated activation do not significantly**
642 **change across inflammation states in the oral mucosa.**

643 **A.** Expression of CD39+ PD-1+ (right) and ICOS+ PD-1+ (left) among all T cell subsets across
644 inflammation (blue, mild; yellow, moderate; red, severely inflamed). No statistical differences

645 within each subset across inflammation. **B.** Representative flow cytometry plots of CD39
646 (BUV615) by PD-1 (BV605) expression (top) and ICOS (BUV737) by PD-1 (BV605) expression
647 (bottom) within CD4 Tconv cells isolated from severely inflamed oral mucosal tissue. **C.** From left
648 to right, expression of Ki67+ and TIM3+ PD-1+ across T cell subsets across inflammation status.
649 No statistical differences within each subset. **D.** Representative flow cytometry plots of Ki67
650 (BV650) expression (top) and TIM3 (BB515) by PD-1 (BV605) expression (bottom) within CD4
651 Tconv cells isolated from moderately inflamed (top) or severely inflamed (bottom) oral mucosal
652 tissue. No significant differences by ordinary one-way ANOVA with Tukey's multiple comparison
653 test.
654
655 **Figure 3: Functional capacity of T cell subsets is maintained in inflamed oral mucosa.**
656 **A.** Within T cell subset, expression of each molecule across mild, moderate, or severely inflamed
657 oral mucosa following 6h PMA/I stimulation. n = 9 mild, 13 moderate, 11 severely inflamed oral
658 mucosa tissues, unless noted based on minimum threshold for analysis of 25 cells. For Tregs, n
659 = 8 mild; n = 11 moderate. No statistical differences across inflammation status for each marker.
660 **B.** Expression of AREG, IFNγ, and IL-2 within each T cell subset; no statical differences across
661 inflammation. **C.** Expression of each molecule within MAIT and γδ T cells. **D.** Representative
662 gating of AREG+ GzmB+ populations within mildly inflamed oral mucosa (left) and co-expression
663 of AREG+ GzmB+ among CD103+ CD8+ resident T cells (right). For MAIT cells, n = 7 mild, n =
664 8 moderate, n = 10 severe; γδ T cells, n = 7 mild, n = 10 severe. No significant differences by
665 ordinary one-way ANOVA with Tukey's multiple comparison test.
666
667 **Figure 4: T cells from lung and decidual-placental interference (DPI) differ based on tissue**
668 **origin regardless of inflammation status**

669 **A.** Among all CD3+ CD45+ cells, frequency of indicated subset within each tissue and disease
670 state. **B.** For conventional subsets (right to left; Tconv, Treg, CD103+ CD8+ and CD103- CD8+),
671 frequency of activation markers by tissue and disease status. Unless noted, n = 4 healthy lung, n
672 = 10 inflamed lung, n = 10 healthy placenta, n = 8 inflamed placenta. Some samples did not meet
673 minimum threshold of 25 cells; for Tregs, n = 3 healthy lung; within CD103+, n = 3 healthy lung
674 for all figure panels. Within one experiment, n = 8 inflamed lung samples for Tconv and Tregs for
675 this and remaining panels. Statistical testing between tissues is excluded from heatmaps. **C.**
676 Frequency of GzmB+ cells among CD8 CD103- across tissue and inflammation state
677 (healthy/mild = blue squares, moderate gingiva = yellow circles, severe/inflamed = red diamonds).
678 **D.** Frequency of TIM3+ Tregs. **E.** Frequency of CTLA-4+ cells among resident CD8 CD103+ cells.
679 Pre-gated as indicated in Supplemental Figure 1 prior to subsetting and single-positive gating. *p
680 < 0.05, **p < 0.01, ***p < 0.001, ****p < 0.0001 by ordinary one-way ANOVA with Tukey's multiple
681 comparison test.
682
683 **Figure 5: Functional capacity of T cells is primarily shaped by tissue location.**
684 **A.** Upon 6hr stimulation with PMA/ionomycin, expression of cytokines and tissue healing markers
685 across T cell subsets in the lung and placenta. Unless noted, n = 4 healthy lung, n = 10 inflamed
686 lung, n = 10 healthy placenta, n = 8 inflamed placenta. For Tconv and Tregs, n = 8 inflamed lung
687 samples for this and subsequent figure panels. Statistical testing between tissues excluded from
688 heatmaps. **B.** Within each T cell subset, expression of IFNγ (left), IL-2 (middle), and IL-17A (right).
689 For all panels, circles = gingiva, upright triangle = lung, upside down triangle = placenta; for this
690 and subsequent figure panels, healthy/mild = blue, moderate gingiva = yellow, severe/inflamed =
691 red. For MAIT cells, n = 3 healthy lung and n = 9 inflamed lung samples. **C.** TNFα expression
692 across tissues in CD4 Tconv (left) and CD8 CD103- (right), pre-gated based on Supplemental
693 Figure 1 scheme. **D.** Frequencies of IFNγ+ IL-2+ across tissues in CD4 Tconv (left) and Tregs

694 (right). *p < 0.05, **p < 0.01, ***p < 0.001, ****p < 0.0001 by ordinary one-way ANOVA with
695 Tukey's multiple comparison test.
696
697 **Figure 6: Functional capacity of T cells across tissues and inflammation state by**
698 **dimensionality reduction analysis**
699 Principal components determined by frequency of positive cells within gates from the following
700 parameters: TIM3, CD39, ICOS, CD25, CD28, CD27, PD1, Ki67, IL1R1, CD137, CD40L, CTLA4,
701 IL-2, IL-22, AREG, IL-17A, IFNγ, GzmB, TNFα, IL-17F. PCA plots of flow cytometry data following
702 6-hour PMA/Ionomycin stimulation from gingiva (pink), lung (green), and placenta (purple) during
703 health (blue) and inflammation (red) organized by tissue type (left) and inflammation status (right)
704 of **A.** CD4 Tconv, **B.** CD8 CD103+, **C.** MAIT cells, **D.** γδ T cells. Moderately inflamed oral mucosa
705 is grouped with inflammation category. Ellipses represent 95% confidence interval.
706
707 **Figure 7: An unsupervised analysis approach to compare the T cell compartment across**
708 **tissues and inflammation.**
709 The following markers were used to develop clusters: CD161, CD39, CCR7, ICOS, CD25, IL-17F,
710 CD28, CD27, CD45RA, PD-1, Ki67, CD69, TIM3, IFNγ, CTLA4, IL-13, IL-22, GzmB, TNFα, IL1R1,
711 CD137, AREG, CD40L, IL-17A, CD45RO, IL-2. **A.** UMAPs of clusters organized by tissue origin
712 and inflammation status. **B.** Bubble plots of expression of each marker within each cluster among
713 Tregs upon stimulation. Resolution = 0.75. **C.** Box plots of frequency of each cluster relative to
714 CD4 Treg counts out of total T cells from each sample. **D.** Stacked bar graphs representing cluster
715 breakdown for individual samples.
716

REFERENCES

1. Sathaliyawala, T., Kubota, M., Yudanin, N., Turner, D., Camp, P., Thome, J.J., Bickham, K.L., Lerner, H., Goldstein, M., Sykes, M., et al. (2013). Distribution and compartmentalization of human circulating and tissue-resident memory T cell subsets. Immunity *38*, 187-197. 10.1016/j.immuni.2012.09.020.
2. Kumar, B.V., Ma, W., Miron, M., Granot, T., Guyer, R.S., Carpenter, D.J., Senda, T., Sun, X., Ho, S.H., Lerner, H., et al. (2017). Human Tissue-Resident Memory T Cells Are Defined by Core Transcriptional and Functional Signatures in Lymphoid and Mucosal Sites. Cell Rep *20*, 2921-2934. 10.1016/j.celrep.2017.08.078.
3. Szabo, P.A., Levitin, H.M., Miron, M., Snyder, M.E., Senda, T., Yuan, J., Cheng, Y.L., Bush, E.C., Dogra, P., Thapa, P., et al. (2019). Single-cell transcriptomics of human T cells reveals tissue and activation signatures in health and disease. Nat Commun *10*, 4706. 10.1038/s41467-019-12464-3.
4. Connors, T.J., Matsumoto, R., Verma, S., Szabo, P.A., Guyer, R., Gray, J., Wang, Z., Thapa, P., Dogra, P., Poon, M.M.L., et al. (2023). Site-specific development and progressive maturation of human tissue-resident memory T cells over infancy and childhood. Immunity *56*, 1894-1909 e1895. 10.1016/j.immuni.2023.06.008.
5. Poon, M.M.L., Caron, D.P., Wang, Z., Wells, S.B., Chen, D., Meng, W., Szabo, P.A., Lam, N., Kubota, M., Matsumoto, R., et al. (2023). Tissue adaptation and clonal segregation of human memory T cells in barrier sites. Nat Immunol *24*, 309-319. 10.1038/s41590-022-01395-9.
6. Wong, M.T., Ong, D.E., Lim, F.S., Teng, K.W., McGovern, N., Narayanan, S., Ho, W.Q., Cerny, D., Tan, H.K., Anicete, R., et al. (2016). A High-Dimensional Atlas of Human T Cell Diversity Reveals Tissue-Specific Trafficking and Cytokine Signatures. Immunity *45*, 442-456. 10.1016/j.immuni.2016.07.007.
7. Niessl, J., Muller, T.R., Constantz, C., Cai, C., Nilsen, V., Rivera Ballesteros, O., Adamo, S., Kammann, T., Mouchtaridi, E., Gao, Y., et al. (2025). Tissue origin and virus specificity shape human CD8(+) T cell cytotoxicity. Sci Immunol *10*, eadq4881. 10.1126/sciimmunol.adq4881.
8. Reina-Campos, M., Monell, A., Ferry, A., Luna, V., Cheung, K.P., Galletti, G., Scharping, N.E., Takehara, K.K., Quon, S., Challita, P.P., et al. (2025). Tissue-resident memory CD8 T cell diversity is spatiotemporally imprinted. Nature *639*, 483-492. 10.1038/s41586-024-08466-x.
9. Traxinger, B.R., Richert-Spuhler, L.E., and Lund, J.M. (2022). Mucosal tissue regulatory T cells are integral in balancing immunity and tolerance at portals of antigen entry. Mucosal Immunol *15*, 398-407. 10.1038/s41385-021-00471-x.
10. Munoz-Rojas, A.R., and Mathis, D. (2021). Tissue regulatory T cells: regulatory chameleons. Nat Rev Immunol *21*, 597-611. 10.1038/s41577-021-00519-w.
11. Miragaia, R.J., Gomes, T., Chomka, A., Jardine, L., Riedel, A., Hegazy, A.N., Whibley, N., Tucci, A., Chen, X., Lindeman, I., et al. (2019). Single-Cell Transcriptomics of Regulatory T Cells Reveals Trajectories of Tissue Adaptation. Immunity *50*, 493-504 e497. 10.1016/j.immuni.2019.01.001.
12. Simon, M., Stuve, P., Schmidleithner, L., Bittner, S., Beumer, N., Strieder, N., Schmidl, C., Pant, A., Gebhard, C., Eigenberger, A., et al. (2024). Single-cell chromatin accessibility and transposable element landscapes reveal shared features of tissue-residing immune cells. Immunity *57*, 1975-1993 e1910. 10.1016/j.immuni.2024.06.015.
13. Gray, J.I., Caron, D.P., Wells, S.B., Guyer, R., Szabo, P., Rainbow, D., Ergen, C., Rybkina, K., Bradley, M.C., Matsumoto, R., et al. (2024). Human gammadelta T cells in diverse tissues exhibit site-specific maturation dynamics across the life span. Sci Immunol *9*, eadn3954. 10.1126/sciimmunol.adn3954.

14. Kammann, T., Cai, C., Sekine, T., Mouchtaridi, E., Boulouis, C., Nilsen, V., Ballesteros, O.R., Muller, T.R., Gao, Y., Raineri, E.J.M., et al. (2024). MAIT cell heterogeneity across paired human tissues reveals specialization of distinct regulatory and enhanced effector profiles. Sci Immunol *9*, eadn2362. 10.1126/sciimmunol.adn2362.
15. Garner, L.C., Amini, A., FitzPatrick, M.E.B., Lett, M.J., Hess, G.F., Filipowicz Sinnreich, M., Provine, N.M., and Klenerman, P. (2023). Single-cell analysis of human MAIT cell transcriptional, functional and clonal diversity. Nat Immunol *24*, 1565-1578. 10.1038/s41590-023-01575-1.
16. Mueller, S.N., Gebhardt, T., Carbone, F.R., and Heath, W.R. (2013). Memory T cell subsets, migration patterns, and tissue residence. Annu Rev Immunol *31*, 137-161. 10.1146/annurev-immunol-032712-095954.
17. Maurice, N.J., Taber, A.K., and Prlic, M. (2021). The Ugly Duckling Turned to Swan: A Change in Perception of Bystander-Activated Memory CD8 T Cells. J Immunol *206*, 455-462. 10.4049/jimmunol.2000937.
18. Lee, H., Jeong, S., and Shin, E.C. (2022). Significance of bystander T cell activation in microbial infection. Nat Immunol *23*, 13-22. 10.1038/s41590-021-00985-3.
19. Sekine, T., Perez-Potti, A., Nguyen, S., Gorin, J.B., Wu, V.H., Gostick, E., Llewellyn-Lacey, S., Hammer, Q., Falck-Jones, S., Vangeti, S., et al. (2020). TOX is expressed by exhausted and polyfunctional human effector memory CD8(+) T cells. Sci Immunol *5*. 10.1126/sciimmunol.aba7918.
20. Maurice, N.J., Berner, J., Taber, A.K., Zehn, D., and Prlic, M. (2021). Inflammatory signals are sufficient to elicit TOX expression in mouse and human CD8+ T cells. JCI Insight *6*. 10.1172/jci.insight.150744.
21. Berg, R.E., and Forman, J. (2006). The role of CD8 T cells in innate immunity and in antigen non-specific protection. Curr Opin Immunol *18*, 338-343. 10.1016/j.coi.2006.03.010.
22. Berg, R.E., Cordes, C.J., and Forman, J. (2002). Contribution of CD8+ T cells to innate immunity: IFN-gamma secretion induced by IL-12 and IL-18. Eur J Immunol *32*, 2807-2816. 10.1002/1521-4141(2002010)32:10<2807::AID-IMMU2807>3.0.CO;2-0.
23. Kambayashi, T., Assarsson, E., Lukacher, A.E., Ljunggren, H.G., and Jensen, P.E. (2003). Memory CD8+ T cells provide an early source of IFN-gamma. J Immunol *170*, 2399-2408. 10.4049/jimmunol.170.5.2399.
24. Chu, T., Tyznik, A.J., Roepke, S., Berkley, A.M., Woodward-Davis, A., Pattacini, L., Bevan, M.J., Zehn, D., and Prlic, M. (2013). Bystander-activated memory CD8 T cells control early pathogen load in an innate-like, NKG2D-dependent manner. Cell Rep *3*, 701-708. 10.1016/j.celrep.2013.02.020.
25. Yajima, T., Nishimura, H., Ishimitsu, R., Yamamura, K., Watase, T., Busch, D.H., Pamer, E.G., Kuwano, H., and Yoshikai, Y. (2001). Memory phenotype CD8(+) T cells in IL-15 transgenic mice are involved in early protection against a primary infection with Listeria monocytogenes. Eur J Immunol *31*, 757-766. 10.1002/1521-4141(200103)31:3<757::aid-immu757>3.0.co;2-q.
26. Whiteside, S.K., Snook, J.P., Williams, M.A., and Weis, J.J. (2018). Bystander T Cells: A Balancing Act of Friends and Foes. Trends Immunol *39*, 1021-1035. 10.1016/j.it.2018.10.003.
27. Kim, J., Chang, D.Y., Lee, H.W., Lee, H., Kim, J.H., Sung, P.S., Kim, K.H., Hong, S.H., Kang, W., Lee, J., et al. (2018). Innate-like Cytotoxic Function of Bystander-Activated CD8(+) T Cells Is Associated with Liver Injury in Acute Hepatitis A. Immunity *48*, 161-173 e165. 10.1016/j.immuni.2017.11.025.
28. McGeachy, M.J., Cua, D.J., and Gaffen, S.L. (2019). The IL-17 Family of Cytokines in Health and Disease. Immunity *50*, 892-906. 10.1016/j.immuni.2019.03.021.
29. Li, J., Casanova, J.L., and Puel, A. (2018). Mucocutaneous IL-17 immunity in mice and humans: host defense vs. excessive inflammation. Mucosal Immunol *11*, 581-589. 10.1038/mi.2017.97.

811 30. Sun, L., Su, Y., Jiao, A., Wang, X., and Zhang, B. (2023). T cells in health and disease. Signal
812 Transduct Target Ther *8*, 235. 10.1038/s41392-023-01471-y.
813 31. Singh, N., Baby, D., Rajguru, J.P., Patil, P.B., Thakkannavar, S.S., and Pujari, V.B. (2019).
814 Inflammation and cancer. Ann Afr Med *18*, 121-126. 10.4103/aam.aam_56_18.
815 32. Turner, D.L., and Farber, D.L. (2014). Mucosal resident memory CD4 T cells in protection and
816 immunopathology. Front Immunol *5*, 331. 10.3389/fimmu.2014.00331.
817 33. Arpaia, N., Green, J.A., Moltedo, B., Arvey, A., Hemmers, S., Yuan, S., Treuting, P.M., and
818 Rudensky, A.Y. (2015). A Distinct Function of Regulatory T Cells in Tissue Protection. Cell *162*,
819 1078-1089. 10.1016/j.cell.2015.08.021.
820 34. Delacher, M., Schmidleithner, L., Simon, M., Stuve, P., Sanderink, L., Hotz-Wagenblatt, A., Wuttke,
821 M., Schambeck, K., Ruhland, B., Hofmann, V., et al. (2024). The effector program of human CD8 T
822 cells supports tissue remodeling. J Exp Med *221*. 10.1084/jem.20230488.
823 35. Konkel, J.E., Cox, J.R., and Wemyss, K. (2024). Bite-sized immunology; damage and microbes
824 educating immunity at the gingiva. Mucosal Immunol *17*, 1141-1150.
825 10.1016/j.mucimm.2024.07.004.
826 36. Kinane, D.F., Stathopoulou, P.G., and Papapanou, P.N. (2017). Periodontal diseases. Nat Rev Dis
827 Primers *3*, 17038. 10.1038/nrdp.2017.38.
828 37. Paprckova, D., Salyova, E., Michalik, J., and Stepanek, O. (2023). Bystander activation in memory
829 and antigen-inexperienced memory-like CD8 T cells. Curr Opin Immunol *82*, 102299.
830 10.1016/j.coi.2023.102299.
831 38. Konecny, A.J., Huang, Y., Setty, M., and Prlic, M. (2024). Signals that control MAIT cell function in
832 healthy and inflamed human tissues. Immunol Rev *323*, 138-149. 10.1111/imr.13325.
833 39. Duhen, R., Fesneau, O., Samson, K.A., Frye, A.K., Beymer, M., Rajamanickam, V., Ross, D., Tran, E.,
834 Bernard, B., Weinberg, A.D., and Duhen, T. (2022). PD-1 and ICOS coexpression identifies tumor-
835 reactive CD4+ T cells in human solid tumors. J Clin Invest *132*. 10.1172/JCI156821.
836 40. Duhen, T., Duhen, R., Montler, R., Moses, J., Moudgil, T., de Miranda, N.F., Goodall, C.P., Blair,
837 T.C., Fox, B.A., McDermott, J.E., et al. (2018). Co-expression of CD39 and CD103 identifies tumor-
838 reactive CD8 T cells in human solid tumors. Nat Commun *9*, 2724. 10.1038/s41467-018-05072-0.
839 41. Simoni, Y., Becht, E., Fehlings, M., Loh, C.Y., Koo, S.L., Teng, K.W.W., Yeong, J.P.S., Nahar, R., Zhang,
840 T., Kared, H., et al. (2018). Bystander CD8(+) T cells are abundant and phenotypically distinct in
841 human tumour infiltrates. Nature *557*, 575-579. 10.1038/s41586-018-0130-2.
842 42. de Goffau, M.C., Lager, S., Sovio, U., Gaccioli, F., Cook, E., Peacock, S.J., Parkhill, J., Charnock-Jones,
843 D.S., and Smith, G.C.S. (2019). Human placenta has no microbiome but can contain potential
844 pathogens. Nature *572*, 329-334. 10.1038/s41586-019-1451-5.
845 43. Briana, D.D., Papaevangelou, V., and Malamitsi-Puchner, A. (2021). The jury is still out on the
846 existence of a placental microbiome. Acta Paediatr *110*, 2958-2963. 10.1111/apa.16048.
847 44. Whiteside, S.A., McGinniss, J.E., and Collman, R.G. (2021). The lung microbiome: progress and
848 promise. J Clin Invest *131*. 10.1172/JCI150473.
849 45. Maher, T.M. (2024). Interstitial Lung Disease: A Review. JAMA *331*, 1655-1665.
850 10.1001/jama.2024.3669.
851 46. Jung, E., Romero, R., Suksai, M., Gotsch, F., Chaemsaithong, P., Erez, O., Conde-Agudelo, A.,
852 Gomez-Lopez, N., Berry, S.M., Meyyazhagan, A., and Yoon, B.H. (2024). Clinical chorioamnionitis
853 at term: definition, pathogenesis, microbiology, diagnosis, and treatment. Am J Obstet Gynecol
854 *230*, S807-S840. 10.1016/j.ajog.2023.02.002.
855 47. Sakuishi, K., Ngiow, S.F., Sullivan, J.M., Teng, M.W., Kuchroo, V.K., Smyth, M.J., and Anderson, A.C.
856 (2013). TIM3(+)FOXP3(+) regulatory T cells are tissue-specific promoters of T-cell dysfunction in
857 cancer. Oncoimmunology *2*, e23849. 10.4161/onci.23849.

858 48. Voo, K.S., Wang, Y.H., Santori, F.R., Boggiano, C., Wang, Y.H., Arima, K., Bover, L., Hanabuchi, S.,
859 Khalili, J., Marinova, E., et al. (2009). Identification of IL-17-producing FOXP3+ regulatory T cells in
860 humans. Proc Natl Acad Sci U S A *106*, 4793-4798. 10.1073/pnas.0900408106.
861 49. Beriou, G., Costantino, C.M., Ashley, C.W., Yang, L., Kuchroo, V.K., Baecher-Allan, C., and Hafler,
862 D.A. (2009). IL-17-producing human peripheral regulatory T cells retain suppressive function.
863 Blood *113*, 4240-4249. 10.1182/blood-2008-10-183251.
864 50. Bamashmous, S., Kotsakis, G.A., Kerns, K.A., Leroux, B.G., Zenobia, C., Chen, D., Trivedi, H.M.,
865 McLean, J.S., and Darveau, R.P. (2021). Human variation in gingival inflammation. Proc Natl Acad
866 Sci U S A *118*. 10.1073/pnas.2012578118.
867 51. Kerns, K.A., Bamashmous, S., Hendrickson, E.L., Kotsakis, G.A., Leroux, B.G., Daubert, D.D.,
868 Roberts, F.A., Chen, D., Trivedi, H.M., Darveau, R.P., and McLean, J.S. (2023). Localized microbially
869 induced inflammation influences distant healthy tissues in the human oral cavity. Proc Natl Acad
870 Sci U S A *120*, e2306020120. 10.1073/pnas.2306020120.
871 52. Dominguez-Villar, M., Baecher-Allan, C.M., and Hafler, D.A. (2011). Identification of T helper type
872 1-like, Foxp3+ regulatory T cells in human autoimmune disease. Nat Med *17*, 673-675.
873 10.1038/nm.2389.
874 53. Wang, J., Ioan-Facsinay, A., van der Voort, E.I., Huizinga, T.W., and Toes, R.E. (2007). Transient
875 expression of FOXP3 in human activated nonregulatory CD4+ T cells. Eur J Immunol *37*, 129-138.
876 10.1002/eji.200636435.
877 54. Walker, M.R., Kasprowicz, D.J., Gersuk, V.H., Benard, A., Van Landeghen, M., Buckner, J.H., and
878 Ziegler, S.F. (2003). Induction of FoxP3 and acquisition of T regulatory activity by stimulated
879 human CD4+CD25- T cells. J Clin Invest *112*, 1437-1443. 10.1172/JCI19441.
880 55. Ziegler, S.F. (2007). FOXP3: not just for regulatory T cells anymore. Eur J Immunol *37*, 21-23.
881 10.1002/eji.200636929.
882 56. Koch, M.A., Tucker-Heard, G., Perdue, N.R., Killebrew, J.R., Urdahl, K.B., and Campbell, D.J. (2009).
883 The transcription factor T-bet controls regulatory T cell homeostasis and function during type 1
884 inflammation. Nat Immunol *10*, 595-602. 10.1038/ni.1731.
885 57. Galant-Swafford, J., Catanzaro, J., Achcar, R.D., Cool, C., Koelsch, T., Bang, T.J., Lynch, D.A., Alam,
886 R., Katial, R.K., and Fernandez Perez, E.R. (2024). Approach to diagnosing and managing
887 granulomatous-lymphocytic interstitial lung disease. EClinicalMedicine *75*, 102749.
888 10.1016/j.eclinm.2024.102749.
889 58. Cao, S., Liu, X., Li, Y., Yang, Y., Cai, X., Cong, S., Li, Z., Li, Y., Hong, Y., Su, Y., et al. (2024). Serum
890 sCD25 is an indicator for rheumatoid arthritis-associated interstitial lung disease. Clin Exp
891 Rheumatol *42*, 633-641. 10.55563/clinexprheumatol/3iqvk3.
892 59. Chen, H., Tang, J., Liang, J., Huang, D., Pan, C., Liu, S., Du, X., and Tao, L. (2023). Clinical association
893 study on the matrix metalloproteinase expression in the serum of patients with connective tissue
894 disease complicated with interstitial lung disease. Arch Rheumatol *38*, 367-374.
895 10.46497/ArchRheumatol.2023.9547.
896 60. Sheu, B.C., Hsu, S.M., Ho, H.N., Lien, H.C., Huang, S.C., and Lin, R.H. (2001). A novel role of
897 metalloproteinase in cancer-mediated immunosuppression. Cancer Res *61*, 237-242.
898 61. Kim, T.S., Silva, L.M., Theofilou, V.I., Greenwell-Wild, T., Li, L., Williams, D.W., Ikeuchi, T.,
899 Brenchley, L., Genomics, N.N., Computational Biology, C., et al. (2023). Neutrophil extracellular
900 traps and extracellular histones potentiate IL-17 inflammation in periodontitis. J Exp Med *220*.
901 10.1084/jem.20221751.
902 62. Dutzan, N., Kajikawa, T., Abusleme, L., Greenwell-Wild, T., Zuazo, C.E., Ikeuchi, T., Brenchley, L.,
903 Abe, T., Hurabielle, C., Martin, D., et al. (2018). A dysbiotic microbiome triggers T(H)17 cells to
904 mediate oral mucosal immunopathology in mice and humans. Sci Transl Med *10*.
905 10.1126/scitranslmed.aat0797.

63. Woodward Davis, A.S., Roozen, H.N., Dufort, M.J., DeBerg, H.A., Delaney, M.A., Mair, F., Erickson, J.R., Slichter, C.K., Berkson, J.D., Klock, A.M., et al. (2019). The human tissue-resident CCR5(+) T cell compartment maintains protective and functional properties during inflammation. Sci Transl Med *11*. 10.1126/scitranslmed.aaw8718.
64. Zielinski, C.E., Mele, F., Aschenbrenner, D., Jarrossay, D., Ronchi, F., Gattorno, M., Monticelli, S., Lanzavecchia, A., and Sallusto, F. (2012). Pathogen-induced human TH17 cells produce IFN-gamma or IL-10 and are regulated by IL-1beta. Nature *484*, 514-518. 10.1038/nature10957.
65. Ginesin, O., Coyac, B.R., Doppelt-Flikshtain, O., Mayer, Y., Gabay, E., Berg, T., Bar-On, Y., and Zigdon-Giladi, H. (2025). Macrophage Depletion Reduces Bone Loss and Alters Inflammatory Responses: A Mouse Peri-Implantitis Model. J Clin Periodontol *52*, 898-906. 10.1111/jcpe.14120.
66. Moutsopoulos, N.M., Konkel, J., Sarmadi, M., Eskan, M.A., Wild, T., Dutzan, N., Abusleme, L., Zenobia, C., Hosur, K.B., Abe, T., et al. (2014). Defective neutrophil recruitment in leukocyte adhesion deficiency type I disease causes local IL-17-driven inflammatory bone loss. Sci Transl Med *6*, 229ra240. 10.1126/scitranslmed.3007696.
67. Misharin, A.V., Morales-Nebreda, L., Reyfman, P.A., Cuda, C.M., Walter, J.M., McQuattie-Pimentel, A.C., Chen, C.I., Anekalla, K.R., Joshi, N., Williams, K.J.N., et al. (2017). Monocyte-derived alveolar macrophages drive lung fibrosis and persist in the lung over the life span. J Exp Med *214*, 2387-2404. 10.1084/jem.20162152.
68. Prasse, A., Pechkovsky, D.V., Toews, G.B., Jungraithmayr, W., Kollert, F., Goldmann, T., Vollmer, E., Muller-Quernheim, J., and Zissel, G. (2006). A vicious circle of alveolar macrophages and fibroblasts perpetuates pulmonary fibrosis via CCL18. Am J Respir Crit Care Med *173*, 781-792. 10.1164/rccm.200509-1518OC.
69. Zhang, C., Cao, J., Xu, M., Wu, D., Li, W., and Chang, Y. (2023). The role of neutrophils in chorioamnionitis. Front Immunol *14*, 1198831. 10.3389/fimmu.2023.1198831.
70. Leelatian, N., Doxie, D.B., Greenplate, A.R., Mobley, B.C., Lehman, J.M., Sinnaeve, J., Kauffmann, R.M., Werkhaven, J.A., Mistry, A.M., Weaver, K.D., et al. (2017). Single cell analysis of human tissues and solid tumors with mass cytometry. Cytometry B Clin Cytom *92*, 68-78. 10.1002/cyto.b.21481.
71. Maurice, N.J., Erickson, J.R., DeJong, C.S., Mair, F., Taber, A.K., Frutoso, M., Islas, L.V., Vigil, A., Lawler, R.L., McElrath, J., et al. (2025). Cytokine and metabolite networks shape T cell residency and functionality at the term human maternal-fetal interface. J Immunol *214*, 2221-2237. 10.1093/jimmun/vkaf093.
72. Mair, F., Erickson, J.R., Frutoso, M., Konecny, A.J., Greene, E., Voillet, V., Maurice, N.J., Rongvaux, A., Dixon, D., Barber, B., et al. (2022). Extricating human tumour immune alterations from tissue inflammation. Nature *605*, 728-735. 10.1038/s41586-022-04718-w.
73. Mair, F., and Tyznik, A.J. (2019). High-Dimensional Immunophenotyping with Fluorescence-Based Cytometry: A Practical Guidebook. Methods Mol Biol *2032*, 1-29. 10.1007/978-1-4939-9650-6_1.
74. Ashhurst, T.M., Marsh-Wakefield, F., Putri, G.H., Spiteri, A.G., Shinko, D., Read, M.N., Smith, A.L., and King, N.J.C. (2022). Integration, exploration, and analysis of high-dimensional single-cell cytometry data using Spectre. Cytometry A *101*, 237-253. 10.1002/cyto.a.24350.
75. Putri, G.H., Howitt, G., Marsh-Wakefield, F., Ashhurst, T.M., and Phipson, B. (2024). SuperCellCyto: enabling efficient analysis of large scale cytometry datasets. Genome Biol *25*, 89. 10.1186/s13059-024-03229-3.
76. Bilous, M., Herault, L., Gabriel, A.A., Teleman, M., and Gfeller, D. (2024). Building and analyzing metacells in single-cell genomics data. Mol Syst Biol *20*, 744-766. 10.1038/s44320-024-00045-6.
77. Liu, X., Song, W., Wong, B.Y., Zhang, T., Yu, S., Lin, G.N., and Ding, X. (2019). A comparison framework and guideline of clustering methods for mass cytometry data. Genome Biol *20*, 297. 10.1186/s13059-019-1917-7.

954 78. Traag, V.A., Waltman, L., and van Eck, N.J. (2019). From Louvain to Leiden: guaranteeing well-
955 connected communities. Sci Rep *9*, 5233. 10.1038/s41598-019-41695-z.
956 79. Levine, J.H., Simonds, E.F., Bendall, S.C., Davis, K.L., Amir el, A.D., Tadmor, M.D., Litvin, O.,
957 Fienberg, H.G., Jager, A., Zunder, E.R., et al. (2015). Data-Driven Phenotypic Dissection of AML
958 Reveals Progenitor-like Cells that Correlate with Prognosis. Cell *162*, 184-197.
959 10.1016/j.cell.2015.05.047.
960 80. Becht, E., McInnes, L., Healy, J., Dutertre, C.A., Kwok, I.W.H., Ng, L.G., Ginhoux, F., and Newell,
961 E.W. (2018). Dimensionality reduction for visualizing single-cell data using UMAP. Nat Biotechnol.
962 10.1038/nbt.4314.

963

Figure 1

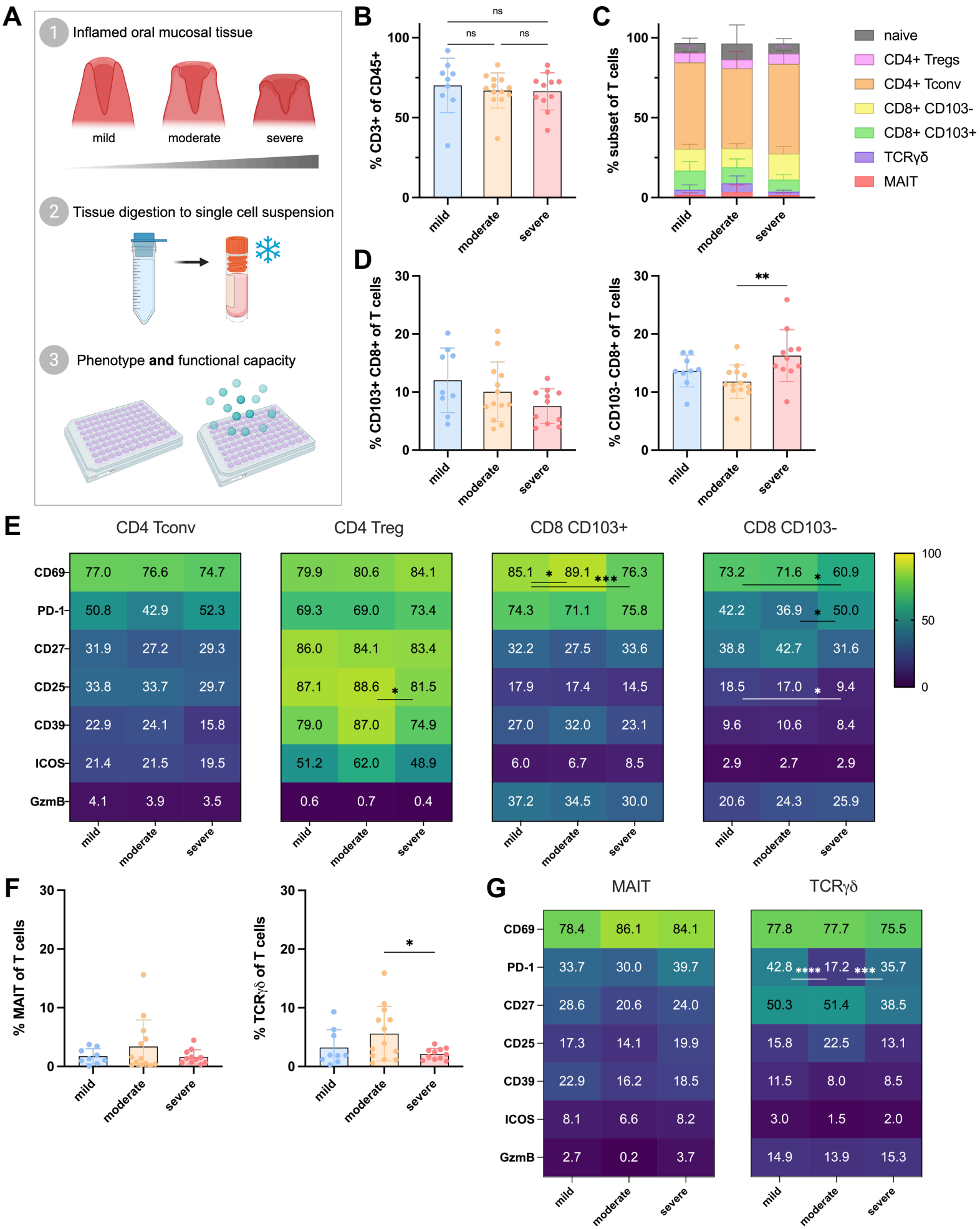
A
1 Inflamed oral mucosal tissue
mild
moderate
severe
2 Tissue digestion to single cell suspension
3 Phenotype and functional capacity
B
% CD3+ of CD45+
ns
ns
ns
mild
moderate
severe
C
% subset of T cells
naive
CD4+ Tregs
CD4+ Tconv
CD8+ CD103-
CD8+ CD103+
TCRγδ
MAIT
D
% CD103+ CD8+ of T cells
% CD103- CD8+ of T cells
**
E
CD4 Tconv
CD4 Treg
CD8 CD103+
CD8 CD103-
CD69
PD-1
CD27
CD25
CD39
ICOS
GzmB
F
% MAIT of T cells
% TCRγδ of T cells
G
MAIT
TCRγδ

Figure 2

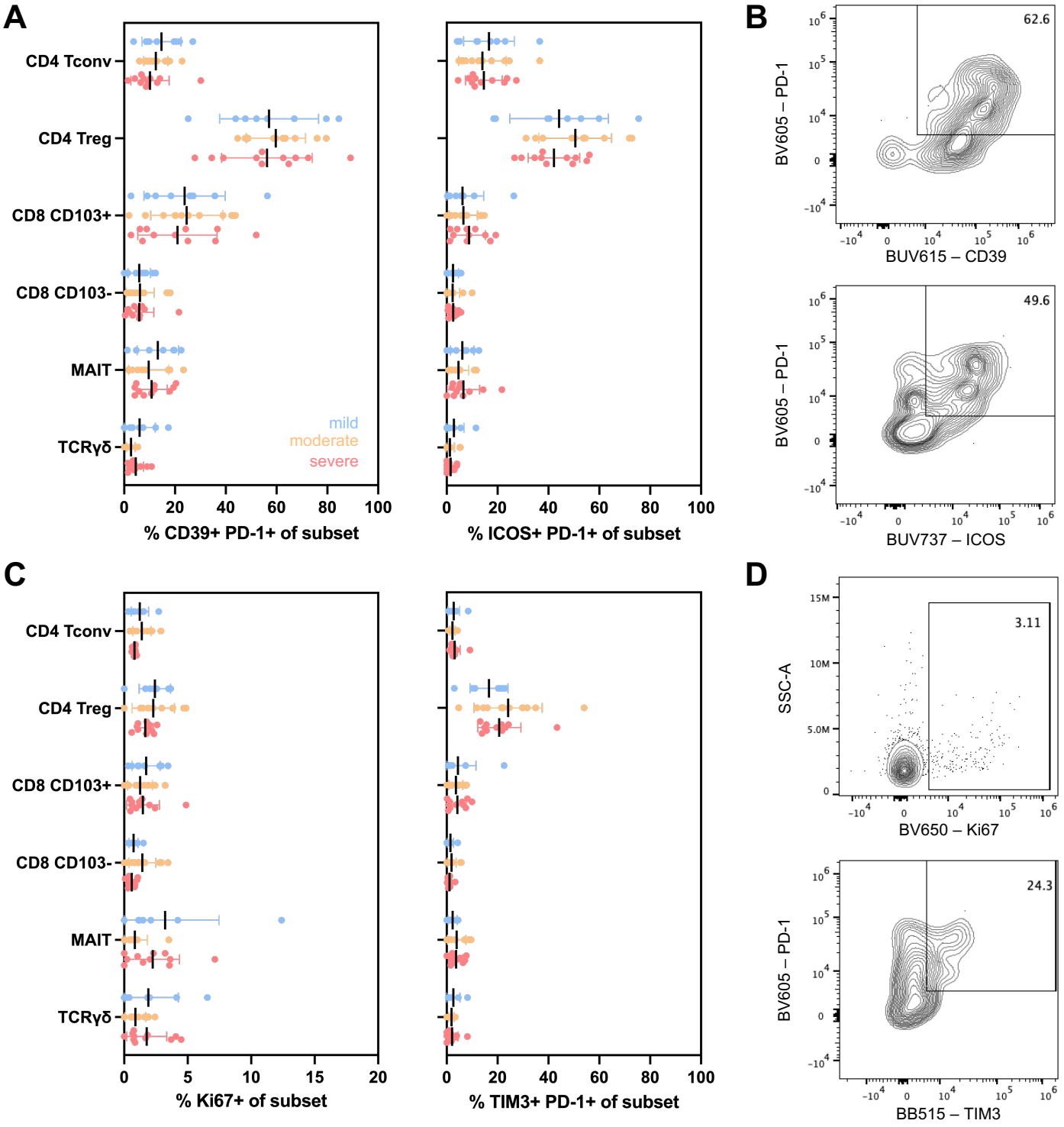
A
CD4 Tconv
CD4 Treg
CD8 CD103+
CD8 CD103-
MAIT
TCRγδ
mild
moderate
severe
% CD39+ PD-1+ of subset
% ICOS+ PD-1+ of subset
B
62.6
BV605 – PD-1
BUV615 – CD39
49.6
BV605 – PD-1
BUV737 – ICOS
C
% Ki67+ of subset
% TIM3+ PD-1+ of subset
D
3.11
SSC-A
BV650 – Ki67
24.3
BV605 – PD-1
BB515 – TIM3

Figure 3

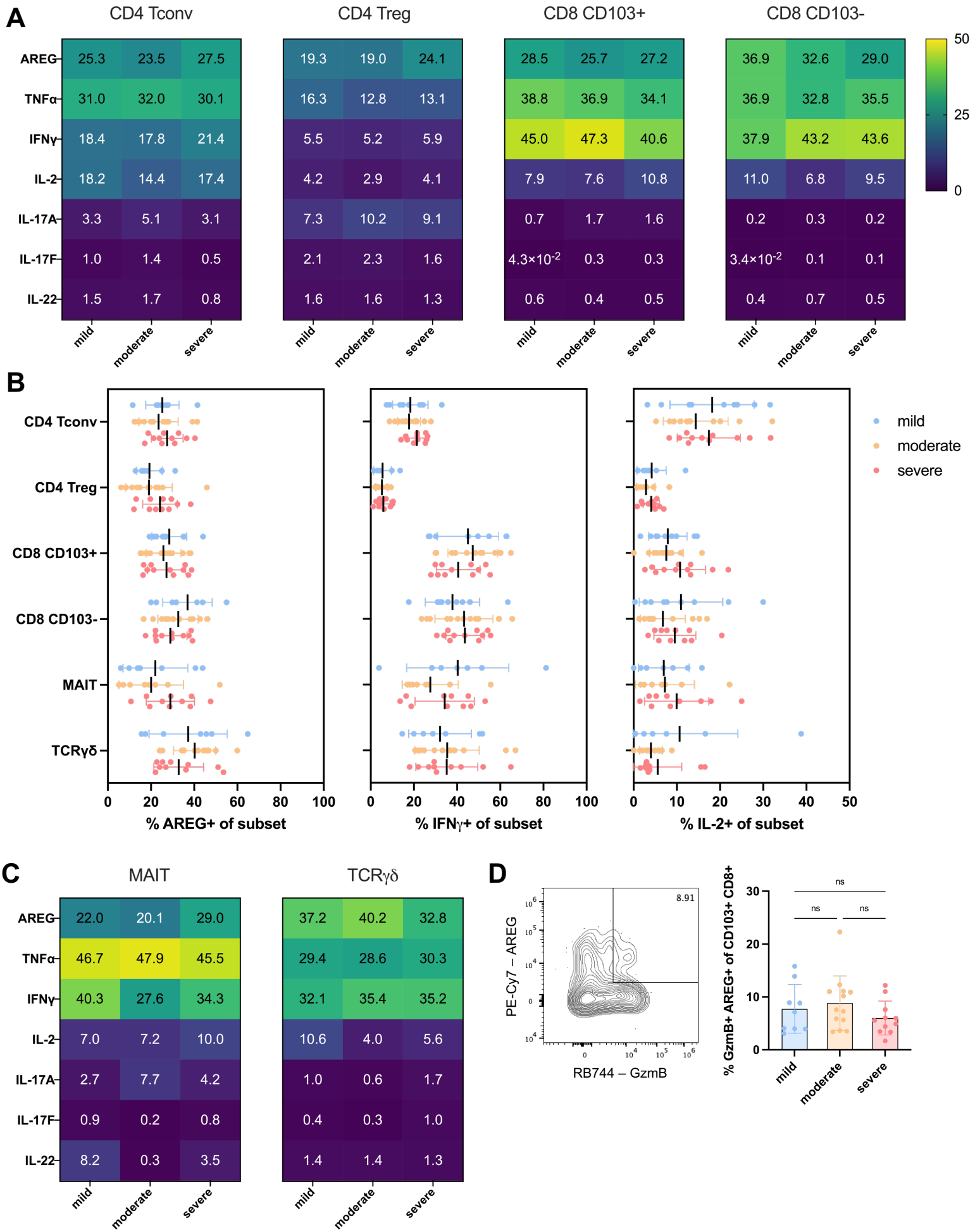
A
CD4 Tconv
CD4 Treg
CD8 CD103+
CD8 CD103-
AREG
TNFα
IFNγ
IL-2
IL-17A
IL-17F
IL-22
mild
moderate
severe
B
CD4 Tconv
CD4 Treg
CD8 CD103+
CD8 CD103-
MAIT
TCRγδ
% AREG+ of subset
% IFNγ+ of subset
% IL-2+ of subset
mild
moderate
severe
C
MAIT
TCRγδ
D
PE-Cy7 – AREG
RB744 – GzmB
8.91
% GzmB+ AREG+ of CD103+ CD8+
ns

Figure 4

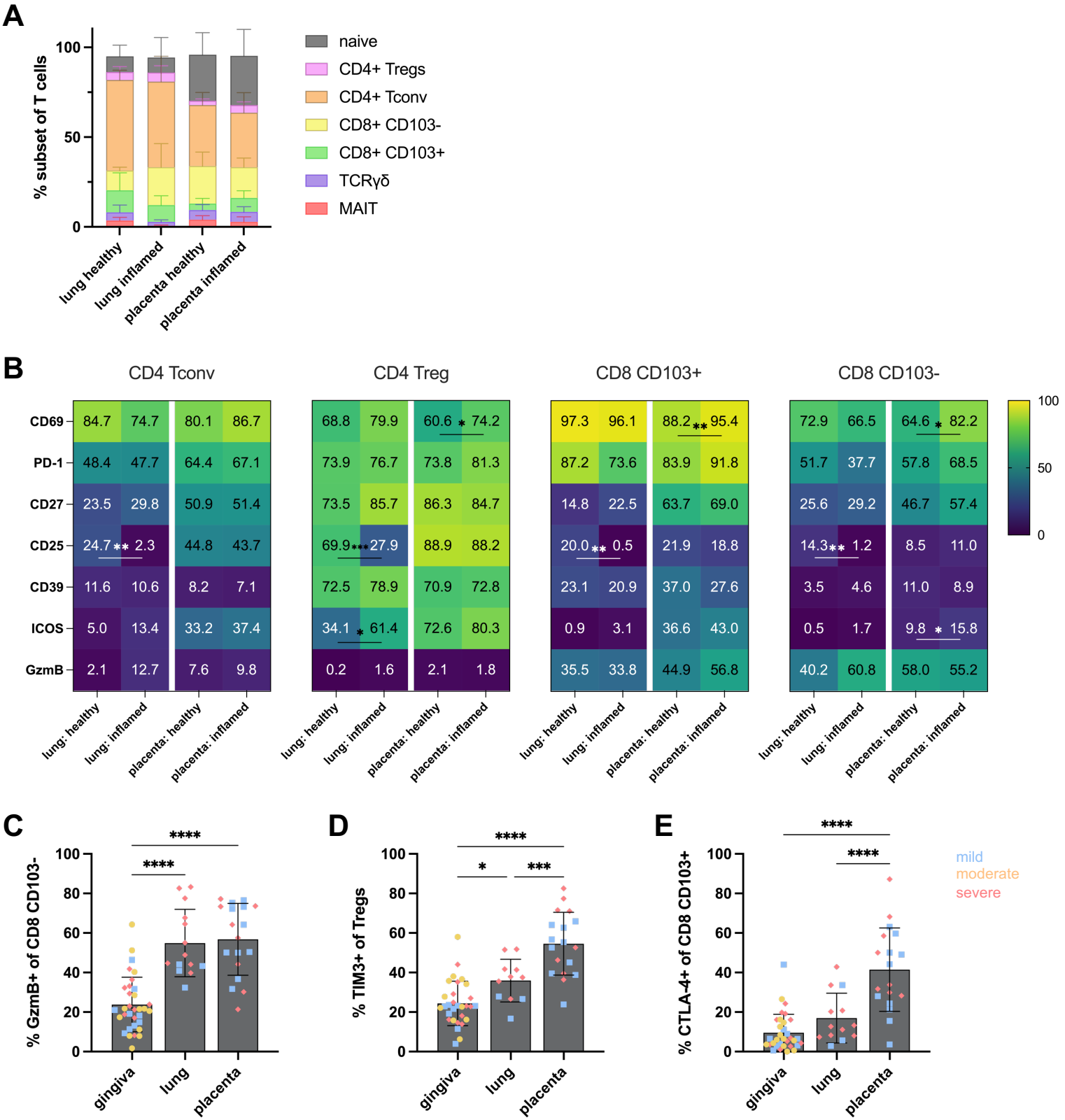
A
% subset of T cells
100
50
0
lung healthy
lung inflamed
placenta healthy
placenta inflamed
naive
CD4+ Tregs
CD4+ Tconv
CD8+ CD103-
CD8+ CD103+
TCRγδ
MAIT
B
CD4 Tconv
CD4 Treg
CD8 CD103+
CD8 CD103-
CD69
PD-1
CD27
CD25
CD39
ICOS
GzmB
lung: healthy
lung: inflamed
placenta: healthy
placenta: inflamed
100
50
0
C
% GzmB+ of CD8 CD103-
gingiva
lung
placenta
D
% TIM3+ of Tregs
E
% CTLA-4+ of CD8 CD103+
mild
moderate
severe

Figure 5

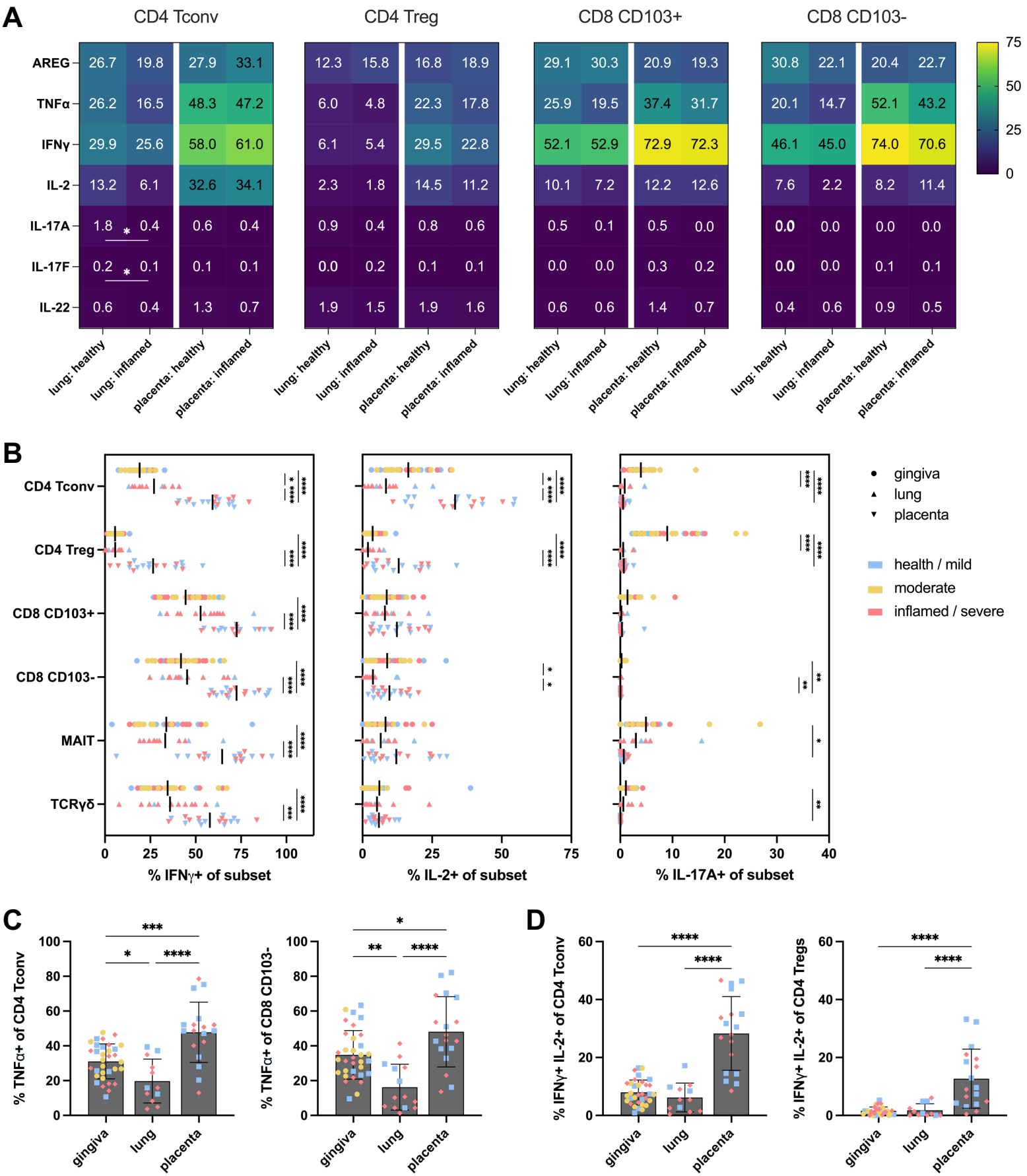
A
CD4 Tconv
CD4 Treg
CD8 CD103+
CD8 CD103-
AREG
TNFα
IFNγ
IL-2
IL-17A
IL-17F
IL-22
lung: healthy
lung: inflamed
placenta: healthy
placenta: inflamed
B
CD4 Tconv
CD4 Treg
CD8 CD103+
CD8 CD103-
MAIT
TCRγδ
% IFNγ+ of subset
% IL-2+ of subset
% IL-17A+ of subset
gingiva
lung
placenta
health / mild
moderate
inflamed / severe
C
% TNFα+ of CD4 Tconv
% TNFα+ of CD8 CD103-
D
% IFNγ+ IL-2+ of CD4 Tconv
% IFNγ+ IL-2+ of CD4 Tregs

Figure 6

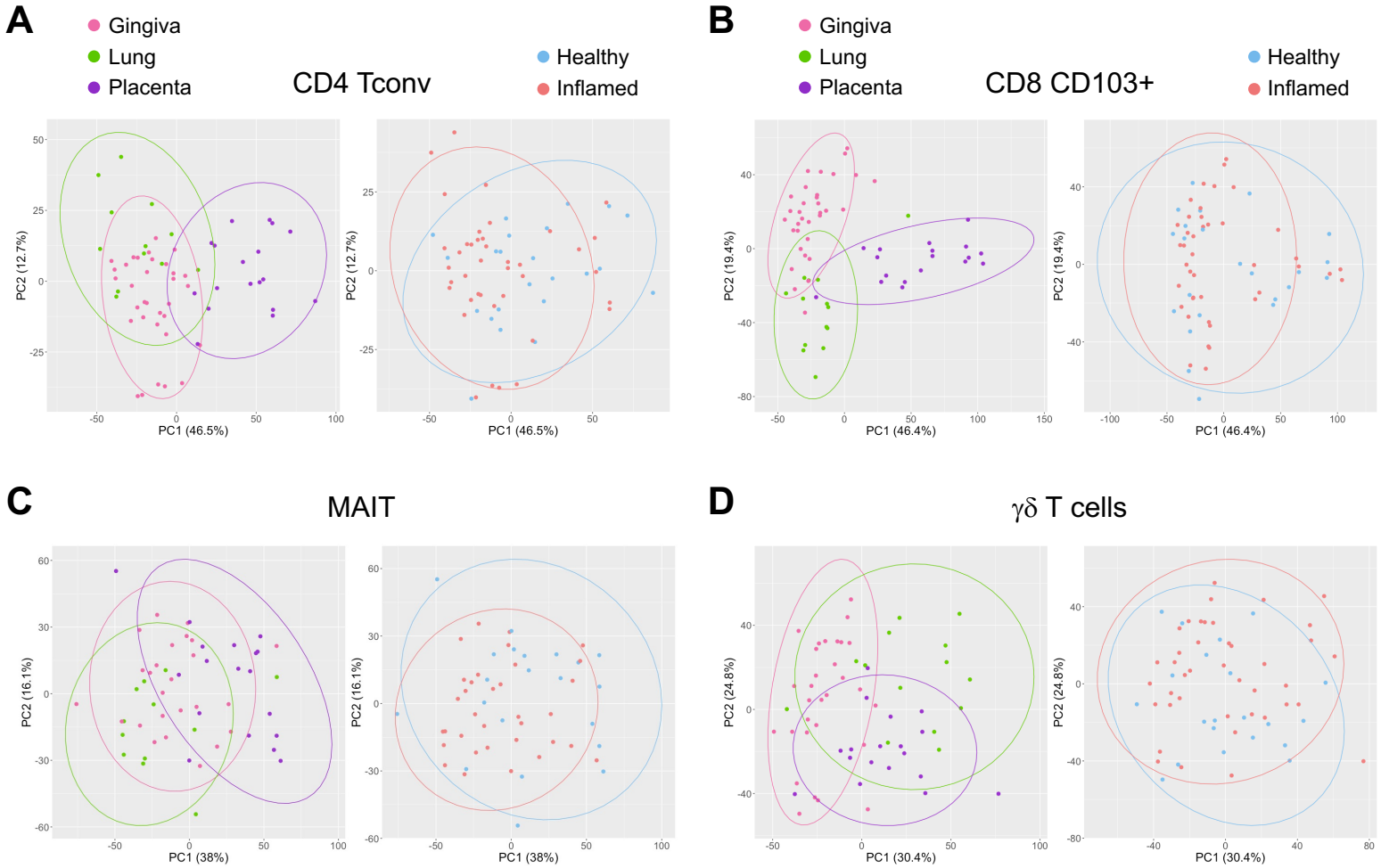
A
Gingiva
Lung
Placenta
CD4 Tconv
Healthy
Inflamed
PC2 (12.7%)
PC1 (46.5%)
B
Gingiva
Lung
Placenta
CD8 CD103+
Healthy
Inflamed
PC2 (19.4%)
PC1 (46.4%)
C
MAIT
PC2 (16.1%)
PC1 (38%)
D
γδ T cells
PC2 (24.8%)
PC1 (30.4%)

Figure 7

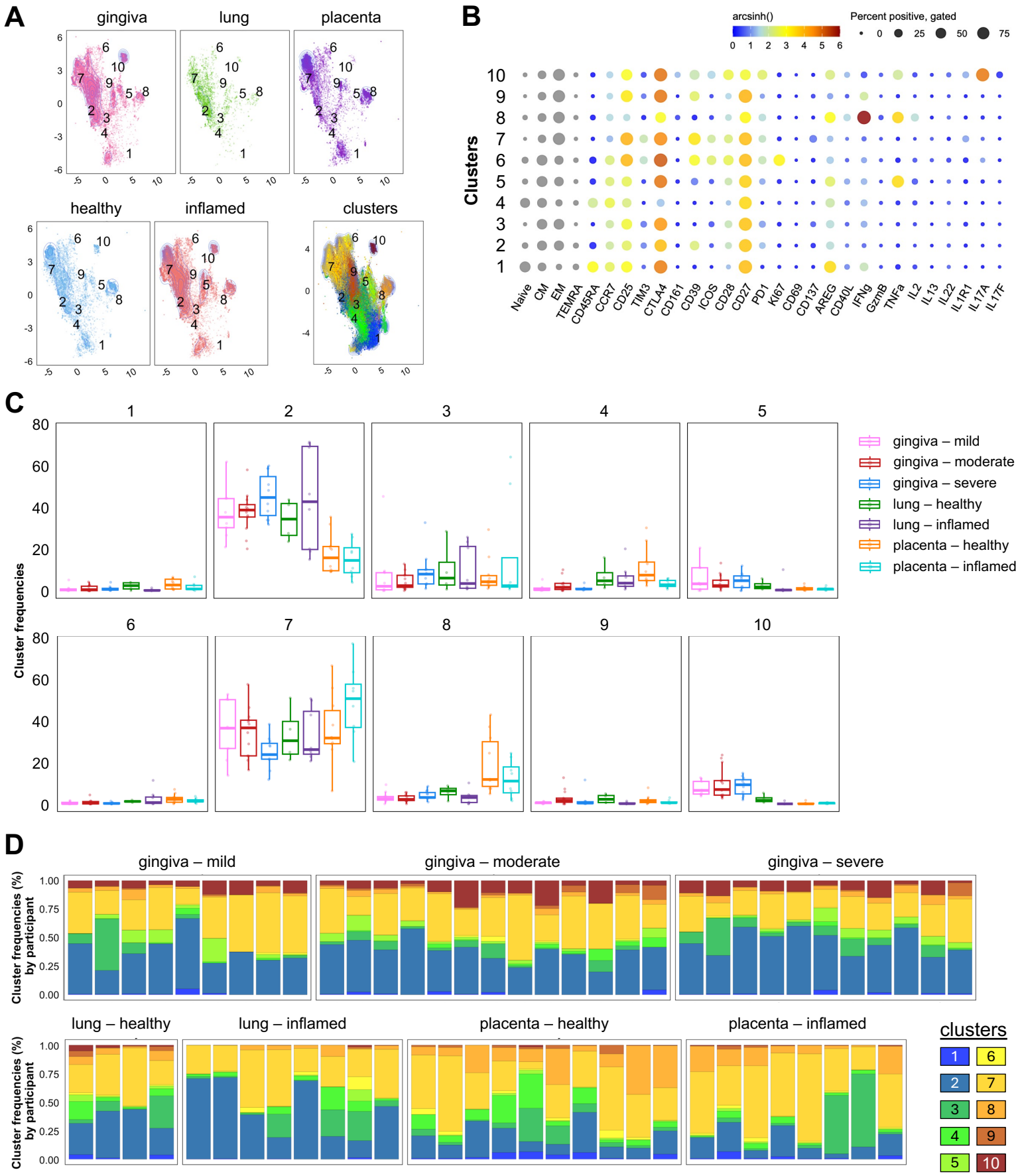
A
gingiva
lung
placenta
healthy
inflamed
clusters
B
arcsinh()
Percent positive, gated
Clusters
Naive
CM
EM
TEMRA
CD45RA
CCR7
CD25
TIM3
CTLA4
CD161
CD39
ICOS
CD28
CD27
PD1
Ki67
CD69
CD137
AREG
CD40L
IFNg
GzmB
TNFa
IL2
IL13
IL22
IL1R1
IL17A
IL17F
C
Cluster frequencies
gingiva – mild
gingiva – moderate
gingiva – severe
lung – healthy
lung – inflamed
placenta – healthy
placenta – inflamed
D
Cluster frequencies (%) by participant
clusters